School of Electronic and Electrical Engineering
FACULTY OF ENGINEERING

UNIVERSITY OF LEEDS

XJEL3875

Project Report

Modelling and Control of Hybrid Energy Storage Integrated Co-phase Power Supply System

Yanshan Xie

SID: *HIDDEN*	Project No. *HIDDEN*
Supervisor: *HIDDEN*	**Assessor:** *HIDDEN*

Abstract

This project firstly identifies shortcomings and possible improvements of the current electrified railway based on actual engineering situations. The project also investigates the current state of research in the field of traction power supply system (TPSS), high-speed railway (HSR) and energy storage system (ESS). In order to mitigate the power quality issues of traditional electrified railway systems and to improve the utilisation of regenerative braking energy (RBE) of high-speed trains, and to reduce the overall energy consumption of the system, this project proposes a novel hybrid energy storage co-phase power supply system (HESCPSS) based on combined co-phase traction power supply system (CTPSS) and hybrid energy storage system (HESS).

Based on the proposed HESCPSS, this project investigates in detail its working principles and operating patterns which embrace all types of load power situations. Besides, along with the HESCPSS, this project proposes a comprehensive control strategy down to power electronic converter switching control up to overall power flow arrangement. This control strategy includes a control method for back-to-back converters within the CTPSS, a control method for half-bridge bi-directional DC-DC converters, a power distribution method within the HESS and a method for overall system coordination. The HESCPSS itself and its control strategy are modelled in MATLAB/Simulink, and the associated simulations and validations are carried out.

It can be demonstrated through simulation outcomes that HESCPSS can effectively achieve comprehensive power quality management while significantly increasing RBE utilisation and rationalising system capacity allocation. The simulation results show that the system operation can sustain the required grid-side power quality under all operating conditions and guarantee excellent dynamic adaptability.

The proposed system structure and control strategy in this project can provide practical technical support for the secure, reliable and efficient operation of electrified railways and facilitate the engineering application of hybrid energy storage integrated co-phase traction power supply systems.

Keywords: Co-phase Traction Power Supply System; Energy Storage System; Regenerative Braking Energy; Real-time Power Control; Power Quality

Acknowledgement

As I look back on my four years of undergraduate study, my heart is full of feelings of clarity. I would like to thank everyone who has accompanied me through these four unusual years at SWJTU-Leeds Joint School, Southwest Jiaotong University.

First of all, I would like to thank all my mentors during this period, who have enlightened me with their virtues and tireless pursuit, who told me to be a competent engineer first, but never to misremember the ambition that followed. That is *Engineers Never Quit.*

Regarding this project, I would particularly like to thank *HIDDEN*, who is also the project supervisor. His meticulous approach and devotedness have always influenced me while participating in *HIDDEN*. The seniors, including *HIDDEN*, have also been very significant in guiding us throughout the year. It was also a pleasure to work with my teammates, especially *HIDDEN*. The successful conduct of the training project has laid the foundation for this final project. I would like to re-appreciate *HIDDEN* for agreeing to *HIDDEN* and giving me the opportunity to accomplish this final project.

I would also like to thank the postgraduate seniors, including *HIDDEN*. During this project, from the proposal writing to the completion, they answered many of my doubts and provided valuable advice on this project's research.

I would also like to highlight my gratitude to my irreplaceable family members who have supported me through my undergraduate studies. I would also like to acknowledge my friends, roommates *HIDDEN*, and a unique individual for their companion-ship and inclusion during this time.

As graduation approaches, I would like to thank and wish all of you mentioned once again. I will take your influence, encouragement and expectations, as well as my enthusiasm for science and engineering, with me as I firmly move on to the subsequent stage of my life.

Contents

List of Figures

List of Tables

Chapter 1

Introduction

In this chapter, the investigation of research on various systems that concerned in this project will be exhibited. In which the characteristics and potential effect of corresponding systems are compared. The reasons of selecting solutions that applied in this project's design are also manifested. Then, the motivation and significance of this project are developed. Finally, the specific objectives of this project are clarified.

1.1 Background and Current Status of Research

1.1.1 Traction Power Supply System

The development and spread of electrified railways have produced leaps and bounds in human society, and electrified railways are substantial electrical load, and their daily consumption of electricity is enormous. However, since their inception, electrified railways have had their share of potential problems, and researchers are continually working to enhance their performance and reduce the impact of electrified railways on other systems. The main problems faced by electrified railways include power quality issues (reactive power, harmonics, negative sequence, voltage fluctuations, flicker) [1, 2], electrical splitting problems, and economic operation problems (transformer utilisation, energy saving).

Specifically for the traction power supply system (TPSS) of high-speed railway (HSR), at present, the 25 kV industrial frequency single-phase AC power supply system is commonly used [3], and its typical structure is shown in Figure 1.1. This type of system has two significant issues.

Power Quality Issues: In today's electrified railways, AC/DC/AC electric locomotives are used in massive volumes, and their PWM rectification technology has resulted in a significant increase in power factor (close to unity) [4]. The electrified railway traction load is a typical single-phase mobile load, and the load of the two supply arms of the traction substation is regularly unbalanced [5]. Through the coupling effect of the traction transformer, negative sequence currents will be generated in the power system, which will cause unbalance in the three-phase power system [6]. The size of the negative sequence current is related to various factors, mainly the power system's capacity, operation mode and traction substation wiring form, locomotive operation mode, and load capacity [7]. Because power quality problems, mainly negative sequence current, can adversely affect transformers, transmission lines and

relay protection within the entire power system, many industry and national standards make requirements for power quality.

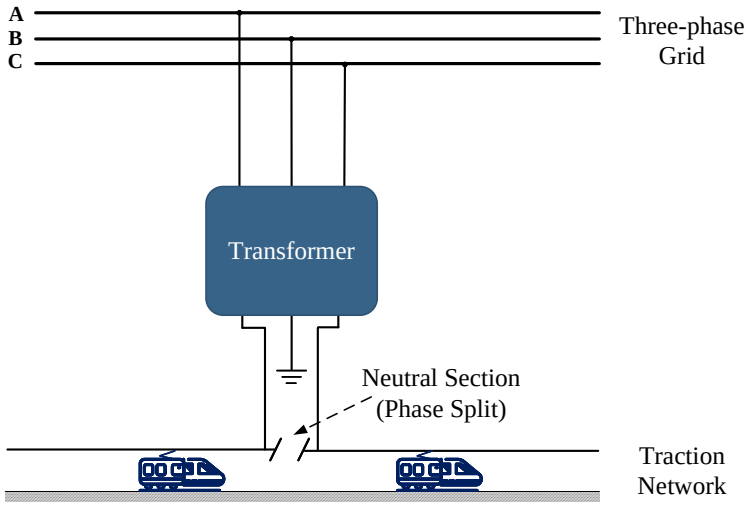

Figure 1.1: Structure of Traditional TPSS

Issues about Neutral Zone: The traditional traction power supply method of phase sequence revolution introduces electrical splitting, as shown in Figure 1.1. The electrical phase separation exists between the two supply arms of the traction substation and between the traction substations and serves as electrical isolation set up every 20 to 30 km. From the circuit point of view, when the train passes through the neutral zone, it is equivalent to momentarily connecting the neutral line of the neutral zone to the circuit and then disconnecting it from the circuit. During this transient process, overvoltage may be generated, which in severe cases may also lead to tripping of the traction substation, affecting the safe operation of the electrified railway and causing significant damages to the railway authorities [8].

In addition, the phase splitting necessitates trains to disconnect the main circuit breaker when passing through the neutral zone, which prevents locomotives from obtaining continuous power, resulting in a loss of speed and limiting the development of HSR. At the same time, frequent opening and closing of circuit breakers by trains can induce arc pulling phenomena, which can burn the electrical equipment and threaten the secure operation of the traction network [9].

Balance Transformer

In order to cope with these problems in conventional TPSS, different researchers have come up with a variety of solutions. Balance transformers are a particular type of transformer used in TPSS to convert a three-phase symmetrical system into a symmetrical two-phase orthogonal system to supply the two supply arms of the traction substation respectively [10]. Due to the special winding or impedance design, the generation of negative sequence currents on the primary side can be effectively suppressed compared to unbalanced transformers, such as V/v transformers [11, 12] and YNvd transformers [13, 14].

However, under actual operating conditions, due to the random nature of the traction load, the power of the two supply arms of the substation cannot be exactly equal, even if the train oper-

ating plan is reasonably arranged, and significant differences often occur. Moreover, balance transformers' ability to suppress negative sequence decreases as the degree of load unbalance between the two arms of the traction substation increases [10]. At the same time, compared to unbalanced transformers, balance transformers do not have high capacity utilisation. They have high consumables, high costs and complex wiring, so there are limitations to using balance transformers to suppress negative sequence currents in TPSS.

Co-phase Traction Supply System

Based on balance transformer technology, Qunzhan Li and his team have developed a three-phase-to-single-phase conversion solution based on active power compensation device (APC) [15], as shown in Figure 1.2. In this solution, one phase of the balance transformer is used to supply the traction network and the another orthogonal phase is linked with a back-to-back APC.

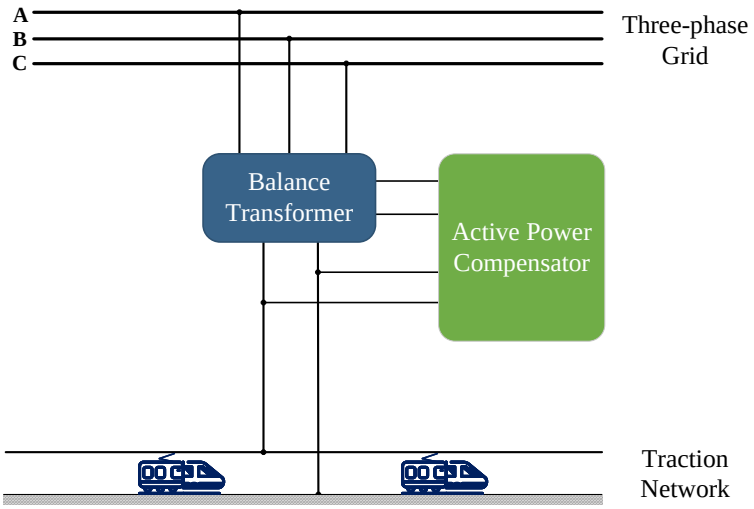

Figure 1.2: Structure of CTPSS

The APC transfers the active power of the load, achieves three-phase balancing on the grid side, eliminates negative sequence currents and also compensates for the reactive power and harmonics of the load. The solution allows for the transformation of an impacting single-phase load with low power factor and high harmonic content into a three-phase symmetrical load that is purely resistive for the power grid and increases the utilisation of the traction transformer [16, 17].

Combined Co-phase Traction Supply System

To reduce the cost of the system, literature [18] proposes a combined co-phase traction power supply system (CTPSS), as shown in Figure 1.3. The single-phase type of combined CTPSS is mainly composed of a traction transformer (TT) and co-phase power supply device (CPD).

Compared to previously mentioned CTPSS, a combined CTPSS can effectively reduce the design capacity of the compensation unit, which also reduces system investment costs. Concurrently, the combined CTPSS can supply trains with power only through a relatively cheap and

stable single-phase traction transformer when the compensation unit is not in operation. These make the TPSS more straightforward and economical and effectively mitigate power quality issues such as negative sequence, reactive power, and harmonics.

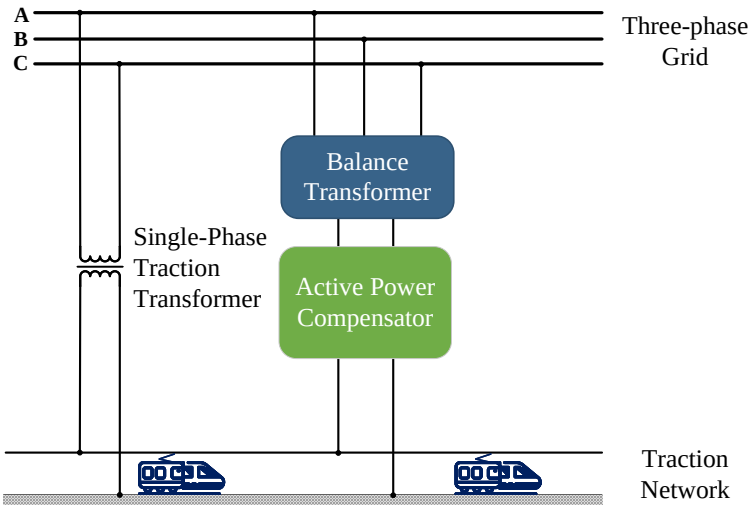

Figure 1.3: Structure of Combined CTPSS

1.1.2 Regenerative Braking Energy

In the braking process, HSR preferentially use regenerative braking as the primary braking method, which contains numerous harmonics and negative sequence components, which will have a severe impact on the reliable operation of the entire power grid when fed back to the grid.

In the field of urban rail transit, the development of regenerative braking energy (RBE) recycling technology represented by the metro is relatively mature. The most widely used mainly include energy-consuming, energy-storage and energy-feeding three utilisation schemes [19]. The energy-consuming utilisation scheme is the most commonly used in urban rail transport [20], with a simple structure and reliable operation. The RBE is dissipated in the form of heat on the energy-consuming resistor, so the energy utilisation rate is low, and the ventilation requirements around the system are high. The energy-storage solution is to store the RBE generated by the vehicle through the energy storage device and release it when the train needs it. This utilisation scheme can incorporate excess energy through the storage device, thus suppressing the grid voltage fluctuation. The Cologne metro in Germany [21], the Madrid metro in Spain [22], the Hokuriku Line substation in Japan [23] and Line 5 of the Beijing metro in China [20] all use the energy storage utilisation scheme. The working principle of the energy-feeding scheme is to return the RBE produced by the trains to the AC grid through a three-phase inverter device and supply it to other power-using equipment [24]. This scheme can effectively reduce the temperature rise in the station caused by the heat emitted from the energy-consuming resistors, thus reducing the investment in cooling equipment, saving energy to a certain extent and improving the utilisation rate of RBE.

Japan successfully developed a commercial RPC system in 2002 and put it into operation on the Shinkansen [25,26]. The operation results show that RPC can effectively transfer the active

power between the two supply arms, reduce the impact of RBE on the grid, and improve the utilisation of RBE to a certain degree.

Wu Songrong's team at Southwest Jiaotong University researched the feeder energy utilisation scheme for electrified railways [27], proposing that RBE be fed back into power supply networks with another voltage level. Ma Xi and Wei Wenjing suggested an energy-storage type utilisation scheme [28], proposing that the RBE generated by electric locomotives be used through energy-storage devices for storage and utilisation, which has more satisfying versatility.

1.1.3 Hybrid Energy Storage System Integration

With the development of technologies such as smart grids, renewable energies and electric vehicles, and the increasing waste of energy from over-generation [29], energy storage system (ESS) and technologies are of great interest to researchers in various fields. The use of ESSs in the TPSS for the RBE generated by HSR can further improve the utilisation of RBE, which has a paramount practical significance.

ESSs store energy via some process and then release it when energy is demanded. Depending on the conversion method, energy storage technologies can be divided into physical, electromagnetic, phase transition and electrochemical energy storage. Different types of energy storage technologies have significant differences in terms of energy density, power density and economics. The articles [30–32] have evaluated several ESSs, and the properties of different systems can be summarised in comparison as presented in Table 1.1.

Table 1.1: Comparison of Properties of Mainstream ESSs

ESS Types	Li-ion Battery	Ni-Cd Battery	Super-capacitor(SC)	Compressed Air (CAES)
Rated Power (MW)	0.1-50	0.1-40	100+	5-300
Energy Density (Wh/kg)	120-200	45-80	10-30	30-60
Self discharge per day	1-5%	0.3%	20-40%	Small
Response Time	$<$1/4 cycle	$<$1/4 cycle	few ms	$\sim$1 hr
Efficiency (%)	78-88	60-80	90+	40-70
Device Cost ($/kWh)	280-4000	600-1200	100-500	2-50
Lifetime (cycles)	$<$1000	2000-2500	$>$100,000	$>$10,000
Maturity	Mature	Outmoded	Developed	Developed

When selecting the type of ESS, the level of its storage performance, power density, impact on the power quality of the original system, control complexity and operating expenses are typically weighed. In combination with the load conditions of the traction system, the ESS integrated into the TPSS needs to meet the following requirements: fast charging and discharging response time and high power density to cope with fast-changing and complex traction loads and power quality requirements; reasonable storage space occupation, charging and discharging efficiency; stable and efficient operation over a long period and installation hardness. Therefore, ESSs based on supercapacitor (SC) and lithium-ion battery (BAT) are considered promising in TPSS.

The concept of hybrid energy storage was first proposed in 2002 and has been theoretically verified. The use of hybrid energy storage system (HESS) can not only integrate the characteristics of different energy storage technologies but also effectively improve the economy of the ESS, which is the current research hotspot of energy storage technology. The BAT and the SC have discernable complementary performance, and the HESS can give full play to their respective advantages, reduce the internal losses of the system, improve the net power output, so that the HESS offers both high dynamic power and large capacity [33].

The real-time allocation of power commands is the primary problem in controlling HESSs, and many scholars have carried out many sorts of research. Ding Ming et al. used a low-pass filtering algorithm to determine the target power value, and by considering the energy storage medium's, the power deviation beyond the target value is allocated between the two energy storage media using fuzzy control theory by considering the state of charge of the energy storage medium [34]; Peng Zhang et al. decompose the unbalanced power of the wind farm using the frequency division technique of wavelet packet decomposition, determine the optimal wavelet packet decomposition layers and frequency division points to separate the high-frequency components, and achieve the power allocation and capacity between different energy storage medium according to the optimisation of annual value of the ESS operation cost [35].

Researchers have proposed a Grey Wolf optimiser-based HESS control scheme for electrified railways [36]. These studies even consider the application of photovoltaic. Some researchers have gone a step further and proposed an overall energy management resolution based on commercial solvers and taking into account uncertainty, based on information-gap decision theory [37].

1.2 Research Motivation and Significance

Focusing on the power quality problems generated by the current high-speed trains of the electrified railway in the traditional TPSS, combined with the current situation that the RBE of high-speed trains cannot be productively utilised, this project attempts to propose a new type of system. Taking full advantages of the combined CTPSS and HESS, this project hopes to suggest a system that can adequately resolve these problems while reducing the overall energy waste and improving the overall system economy, achieving a win-win outcome for both the railway authorities and the power supply grid side.

Not only is it necessary to design a system, but it is also necessary to design a corresponding control method. The overall control strategy should be adaptable and flexible to the diverse operating conditions of the system, and the control method should secure that the system can be operated at a reasonable cost while taking into account the working life of the individual components. Ultimately, the strategy should also allow real-time control in the field in real systems.

The realisation of the proposed method is of paramount significance for the secure, reliable and efficient operation of electrified railways, especially for heavy load and high-speed railways.

1.3 Objectives

Based on the research above, this project intends to design a comprehensive method for modelling and control the hybrid energy storage co-phase power supply system (HESCPSS) which applied to HSR. The HESCPSS are expected to enhance the RBE utilisation and ease the power quality issues. For the proposed system to be able to accomplish the following objectives:

- It must be capable of handling the problems of reactive power, harmonics, overvoltage, and three-phase unbalance in conventional TPSS in an integrated manner.
- It is essential to be able to make the best possible use of the massive amount of RBE generated by high-speed trains, and at the same time to digest this energy intelligently.
- It is required to attach the HESS to the TPSS in a reasonable practice and make full use of its different energy storage units while fairly sustaining its working life.
- It has to be competent on controlling the power electronic converters in the various parts of the system in real-time to ensure desired adequate power flow.
- It is expected to save costs in all aspects of the system in terms of overall control strategy while also providing a reasonable range of adaptation adjustments for the actual operator.

To accomplish these objectives above, the achievement of the following specific tasks is expected:

- Derive and justify the principle of a system that meet the above requirements;
- Propose and depict a viable overall system structure;
- Design every possible operating pattern of the proposed system, together with a performance analysis;
- Design and describe an overall control strategy that takes into account both the lower-level controller control approach and the higher-level power flow design;
- Build an accurate model of the system in MATLAB/Simulink;
- Implement the control strategy in MATLAB/Simulink;
- Verify the functionality of the various parts of the system and then assess the validity of the control strategy on the system using simulations;
- Evaluate the resulting power quality and the efficacy of HESCPSS based on the simulation results and actual intra-day data of substations.

Chapter 2

Principles of Hybrid Energy Storage Co-phase Power Supply System

As discussed in the previous chapters, the combined CTPSS and HESS have been chosen for this project due to their tremendous advantages in terms of economy and practicality. In this chapter, the structure, operating principle of the combined CTPSS and HESS are discussed separately, and eventually, the topology of the HESCPSS is defined.

2.1 Combined Co-phase Traction Power Supply System

2.1.1 Structure of Combined CTPSS

Differing from conventional split-phase TPSS, the CTPSS has identical voltage phases in each supply arm and removes phase splitting. This improvement makes it possible to supply trains continuously while alleviating negative sequence currents and power quality problems.

Also distinct from the usual CTPSS, the combined CTPSS improves the overall system economy by introducing a single-phase TT and combining it with a balance transformer of different wiring forms while allowing a more rational arrangement of the capacity of the co-phase supply device units. For the specific application of this project, the combined CTPSS will use a single-phase compensation device rather than a three-phase one, which led to a further reduction in overall costs and installation space. Combined CTPSS implies that the compensation devices will be connected to both sides of single-phase transformers in some form.

The structure of CTPSS investigated in this project is presented in Figure 2.1, which also illustrates the connection topology of the system. It can be found that the combined CTPSS comprises the main plain single-phase TT and a CPD, where the CPD consists of a high-voltage matching transformer (HMT), an AC-DC-AC converter (ADA) and a traction matching transformer (TMT).

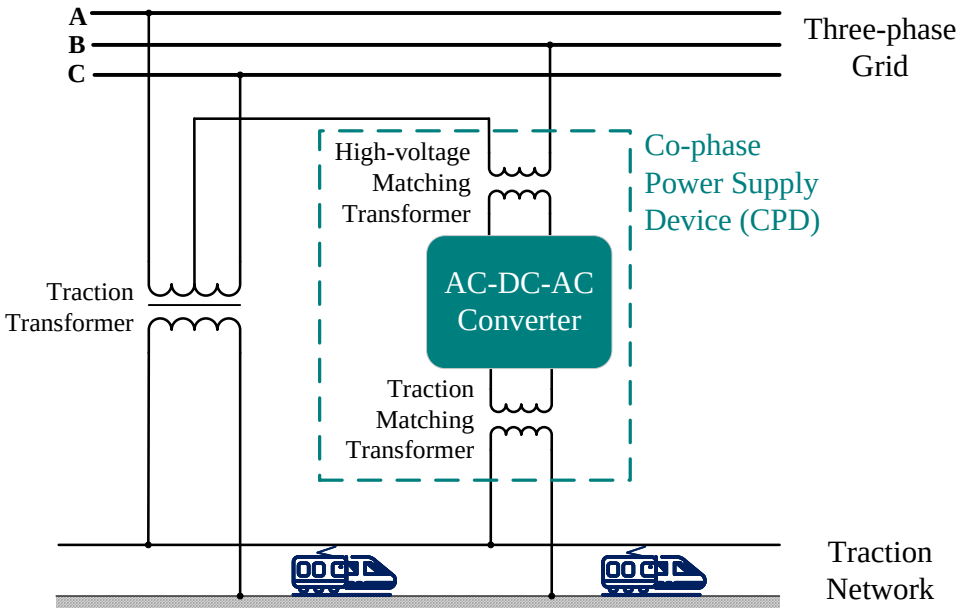

Figure 2.1: Structure of Proposed Combined CTPSS

Traction Transformer (TT) and High-voltage Matching Transformer (HMT)

The primary side of the TT is connected to phases A and C of the three-phase grid at both ends, with the secondary side grounded at one end and connected to the traction bus at the other. The primary side of the HMT is connected to phase B of the grid, the other end is connected to the middle tap of the TT , and the secondary side is attached to the ADA. TT was introduced to match the correct voltage to the traction network, and HMT was introduced mainly to decrease the access voltage to the ADA in order to reduce the expense of the ADA. Considering the TT and HMT coincidentally, one can discover that this particular arrangement forms an inequilateral Scott transformer. Overall, it appears to be a balanced transformer from the point of view of the three-phase grid.

AC-DC-AC converter (ADA)

As shown in Figure 2.2, a general ADA, sometimes called power flow controller, can be regarded as two single-phase and independently controlled H-bridge converters. The structure of the ADA allows it to regulate the active power flow between the two terminals, while the elasticity of its structure, with the appropriate control method, allows it to absorb harmonics produced by the load and compensate the reactive power.

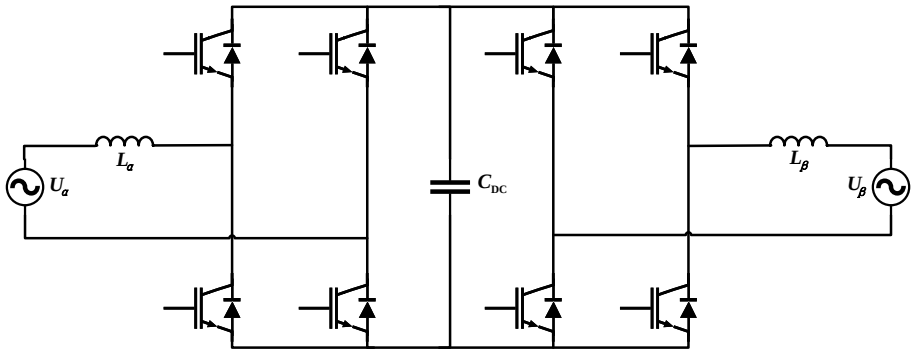

Figure 2.2: Schematic of General ADA

For either end of an H-bridge ADA with this topology, the converter can be equated to a Boost DC-DC converter by analysing the behaviour of the converter in transients [17]. Such a structure introduces a critical limitation that the voltage on the DC link cannot be less than the voltage on the AC side, as shown by the relationship Equation 2.28. This restriction makes it inevitable that the voltage on the DC link is designed to be higher. Consequently, a cascaded H-bridge is introduced.

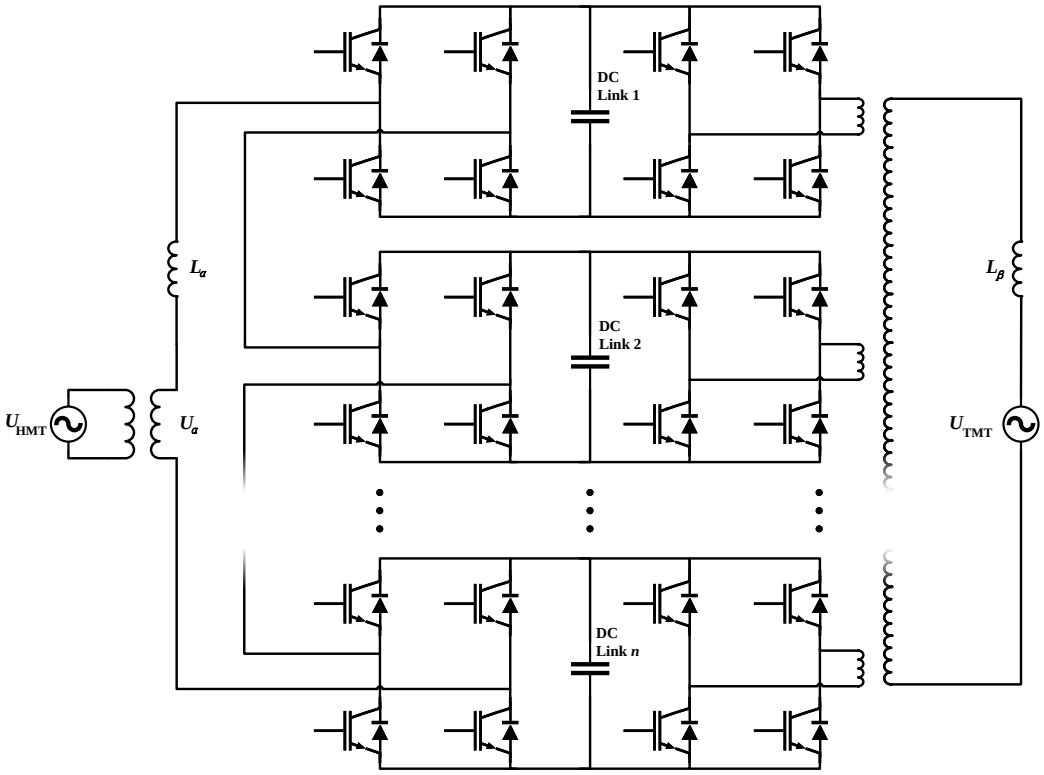

Figure 2.3: Schematic of Cascaded H-bridge CPD

For the cascaded design, the DC link voltage is reduced, the AC side voltage harmonic distortion is attenuated, and the switching frequency of the H-bridge switching devices can be further reduced to reduce converter power losses [38]. Thus, in this project, the ADA comprises several cascaded H-bridge converters as illustrated in Figure 2.3. It is worth to emphasis that in

this project, the HMT side of the ADA is defined as the α phase, and the TMT side is referred to as the β phase.

Traction Matching Transformer (TMT)

Finally, the β phase of the ADA is connected to the TMT, a transformer used to match the voltage between the AC side of the ADA and the traction network. So the traction load can be powered by both the TT and the CPD, and the RBE can be fed back through both the TT and the CPD.

2.1.2 Operating Principle of Combined CTPSS

Besides adjusting the voltage, the arrangement of transformers allows voltages on the secondary side of the TT (U_T) and the primary side of HMT (U_{HMT}) to have a $90°$ phase difference. Their relationship with the three-phase grid is displayed in Figure 2.4.

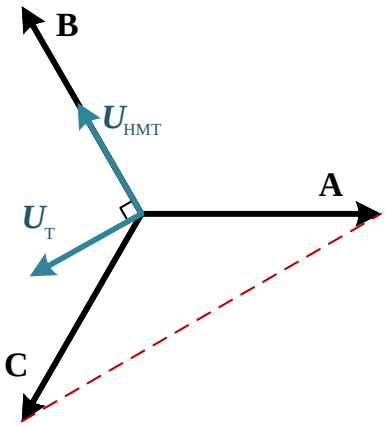

Figure 2.4: Phasor Diagram of Voltages in Proposed CTPSS

Note that the phases of U_{T} and U_{TMT} are identical. Thus, the voltages at two AC terminals of the ADA (U_α,U_β) also have a phase difference of $90°$. Thus, the instantaneous voltages can be defined as:

$$u_{\mathrm{T}}(t) = u_{\mathrm{TMT}}(t) = \sqrt{2}U_{\mathrm{T}}\sin(\omega t) \tag{2.1}$$

$$u_{\mathrm{HMT}}(t) = \sqrt{2}U_{\mathrm{HMT}}\sin(\omega t - \frac{\pi}{2}) \tag{2.2}$$

And it is assumed that traction load current:

$$\begin{aligned} i_L(t) &= \sqrt{2}I_1\sin(\omega t + \varphi_1) + \sum_{n=2}^{\infty}\sqrt{2}I_n\sin(n\omega t + \varphi_n) \\ &= \sqrt{2}I_p\sin(\omega t) + \sqrt{2}I_q\cos(\omega t) + \sum_{n=2}^{\infty}\sqrt{2}I_n\sin(n\omega t + \varphi_n) \\ &= i_{Lp}(t) + i_{Lq}(t) + i_{Lh}(t) \end{aligned} \tag{2.3}$$

where the I_p, I_q are the RMS values of active and reactive current components at fundamental frequency, and $i_{Lp}(t)$, $i_{Lq}(t)$ are their instantaneous value. I_n is the RMS value of n-th harmonic current components, and $i_{Ln}(t)$ is the instantaneous value.

Then, the load power:

$$p_L(t) = u_{\mathrm{T}}(t) i_L(t) \tag{2.4}$$

The load is powered by both TT and TMT and their outputs contain only active power. Thus, the supplying power:

$$p_S(t) = u_{\mathrm{T}}(t) i_{\mathrm{T}}(t) + u_{\mathrm{TMT}}(t) i_{\mathrm{TMT}}(t) \tag{2.5}$$

Note that the energy is conservative over a period:

$$\int_0^T p_S(t)\mathrm{d}t = \int_0^T p_L(t)\mathrm{d}t \tag{2.6}$$

In desired case, the three-phase balance can be fully achieved, and harmonics are fully compensated when:

$$i_{\mathrm{T}}(t) = \frac{\sqrt{2}}{2} I_p \sin(\omega t) \tag{2.7}$$

$$i_{\mathrm{HMT}}(t) = \frac{\sqrt{2}}{2} I_p \sin(\omega t - \frac{\pi}{2}) \tag{2.8}$$

$$i_{\mathrm{TMT}}(t) = \frac{\sqrt{2}}{2} I_p \sin(\omega t) + \sqrt{2} I_q \cos(\omega t) + \sum_{n=2}^{\infty} \sqrt{2} I_n \sin(n\omega t + \varphi_n) \tag{2.9}$$

Thus, the combined CTPSS provided an outstanding power quality from the perspective of three-phase grid. And in this case, defining traction load power S_L, the power provided by TT S_{T}, the throughput power of the CPD $S_{\mathrm{HMT}} = S_{\mathrm{TMT}}$, one can derive that:

$$S_L = S_T + S_{\mathrm{HMT}} \tag{2.10}$$

Since the balanced connection of transformers is set, the negative sequence power S^-:

$$S^- = S_T - S_{\mathrm{HMT}} \tag{2.11}$$

Supposing that the short-circuit capacity of grid connection S_{sc}, the three-phase unbalance factor ε_u can be indicated as

$$\varepsilon_u = \frac{S^-}{S_{\mathrm{sc}}} \times 100\% \tag{2.12}$$

Then, in desired case, following critical condition can be obtained:

$$S_\varepsilon = S^- = S_T - S_{\mathrm{HMT}} \tag{2.13}$$

From Equation 2.13 and Equation 2.10:

$$\begin{bmatrix} S_\varepsilon \\ S_L \end{bmatrix} = \begin{bmatrix} 1 & -1 \\ 1 & 1 \end{bmatrix} \begin{bmatrix} S_T \\ S_{\mathrm{HMT}} \end{bmatrix} \tag{2.14}$$

It can be found with linear transformations:

$$\begin{bmatrix} S_T \\ S_{\mathrm{HMT}} \end{bmatrix} = \frac{1}{2} \begin{bmatrix} 1 & 1 \\ -1 & 1 \end{bmatrix} \begin{bmatrix} S_\varepsilon \\ S_L \end{bmatrix} \tag{2.15}$$

Associating Equation 2.10 and Equation 2.11, the compensation quantity of negative sequence S^-_{HMT}:

$$S^-_{\mathrm{HMT}} = S_L - S^- = 2S_{\mathrm{HMT}} \tag{2.16}$$

Thus, it can be found that the maximum compensation capability of CPD is two times as much as the power capacity of CPD [39]. Overall, the CPD has beneficial contribution to the total load capacity, and alleviates hazards of negative sequence.

2.1.3 Operating Principle of AC-DC-AC Converter

The control methods for ADA in CPD, a crucial part of CTPSS, are discussed in this subsection. In previous chapters, ADA was considered as two single-phase back-to-back converters with a common DC connection. Generally speaking, the ADA topology can be considered as two symmetrical converters, which can be controlled separately. If the two H-bridges in the ADA are recognised as two independently controllable voltage sources, based on Figure 2.2, the equivalent circuit of the ADA can be obtained, as illustrated in Figure 2.5.

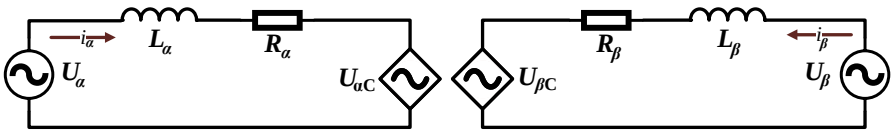

Figure 2.5: Equivalent Circuit of ADA

When the ADA is in regular operation, the DC link should ensure a relatively stable voltage U_{DCref}. When the DC link is not connected to other devices, i.e. when the DC link contains only one capacitor, the active power of the converter on both sides should be balanced, $P_{\alpha\mathrm{C}} = P_{\beta\mathrm{C}}$. Since it is assumed that the two sides of the converter are symmetrical and independently controlled structures, this section only discusses one side for analysis rather than both sides concurrently.

According to Kirchhoff's voltage law, the equation for the loop can be obtained as:

$$U_\alpha = L_\alpha \frac{\mathrm{d}I_\alpha}{\mathrm{d}t} + R_\alpha I_\alpha + U_{\alpha\mathrm{C}} \tag{2.17}$$

Assume that $U_{\alpha\mathrm{C}}$ has a leading phase angle φ of U_α:

$$\dot{U}_\alpha = U_\alpha e^{j0} \tag{2.18}$$

$$\dot{U}_{\alpha\mathrm{C}} = U_{\alpha\mathrm{C}} e^{j\varphi} \tag{2.19}$$

Therefore, the current in this loop:

$$\dot{I}_\alpha = \frac{\dot{U}_\alpha - \dot{U}_{\alpha\mathrm{C}}}{R_\alpha + \omega L_\alpha} \tag{2.20}$$

Then, it can be assumed that the reactance of the inductor is much greater than the equivalent resistance ($\omega L_\alpha \gg R_\alpha$). Applying Euler's formula, the apparent power on the grid side can be obtained:

$$S_\alpha = \dot{U}_\alpha \dot{I}_\alpha^\star = -\frac{U_\alpha U_{\alpha\mathrm{C}} \sin\varphi}{\omega L_\alpha} + j\frac{U_\alpha(U_\alpha - U_{\alpha\mathrm{C}}\cos\varphi)}{\omega L_\alpha} \tag{2.21}$$

In this way, the active and reactive power exchanged by the converter with the grid can be expressed as:

$$P_\alpha = -\frac{U_\alpha U_{\alpha\mathrm{C}} \sin\varphi}{\omega L_\alpha} \tag{2.22}$$

$$Q_\alpha = \frac{U_\alpha(U_\alpha - U_{\alpha\mathrm{C}}\cos\varphi)}{\omega L_\alpha} \tag{2.23}$$

Not only that, but by distinguishing the sign of the phase difference, two operating conditions on this side of the converter can be concerned. Figure 2.6 shows the phase vector diagrams for these two operating conditions, respectively.

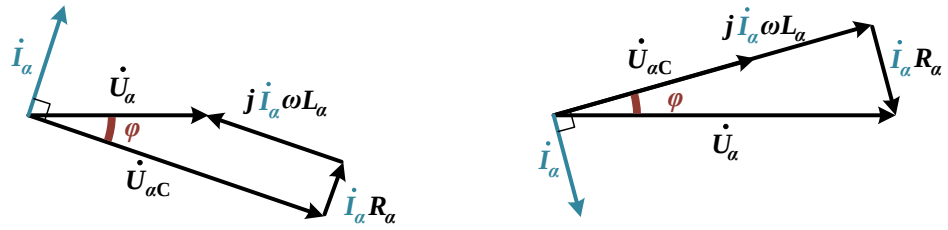

(a) Capacitive Condition (b) Inductive Condition

Figure 2.6: Phasor Diagrams of ADA

Capacitive Condition: As indicated in Figure 2.6(a), when $\varphi < 0$, $U_{\alpha\mathrm{C}}$ lags behind U_α. Therefore, $P_\alpha > 0$, the converter on this side works in rectifier mode and active power flows from the AC side to the DC side.

Inductive Condition: Corresponding to the previous condition, as indicated in Figure 2.6(b), when $\varphi > 0$, $U_{\alpha\mathrm{C}}$ ahead of U_α. Therefore, $P_\alpha < 0$, the converter on this side works in inverter mode and active power flows from the DC side to the AC side.

Based on the Equation 2.23, one can notice that the amount of active power P_α and reactive power Q_α can be adjusted by varying the phase angle and amplitude of $U_{\alpha\mathrm{C}}$. When the value of Q_α is close to 0, excellent reactive power compensation can be achieved. Moreover, although only the performance of the converter at the fundamental frequency has been examined so far, these conclusions can be extended to higher harmonics.

2.2 Hybrid Energy Storage System

2.2.1 Structure of HESS

In the description of the structure of the CTPSS in the previous section, reference was made to the DC link in the ADA. This DC link usually contains only a suitable capacitor, allowing

energy to flow between the α and β phases.

There have been researches focused on combining CTPSS with energy storage system, and such combination is achieved through utilising DC links in ADA. In this project, the HESS is coupled on the DC link, and its structure is manifested in Figure 2.7. As previously discussed, the energy storage devices in the HESS in this project consist mainly of several SC arrays and lithium-ion BAT arrays. Also, in order to ensure stable and reliable energy management capabilities, these arrays of energy storage devices are attached to the DC link in the ADA via a number of independent bi-directional DC-DC converters.

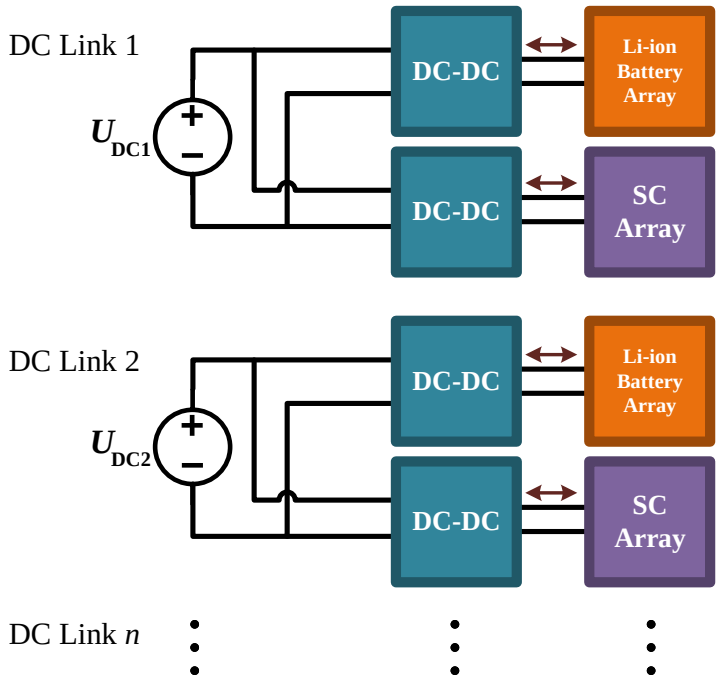

Figure 2.7: Structure of HESS

It is essential to note that this project focuses on the energy management of HESS and the practical integration with combined CTPSS rather than on the HESS energy storage technology itself. Therefore, the project will not focus on the properties of the energy storage mediums themselves.

The focus of integrating the HESS into the combined CTPSS, consequently, falls on the design of the bi-directional DC-DC converter. The DC link of the ADA is intended to be maintained near the reference voltage at all times, while the port voltage of the energy storage array changes with its State-Of-Charge (SOC) and operating conditions. Also, with this converter, the HESS must be flexibly and accurately controlled to absorb and release energy. The DC-DC converter in the form of a half-bridge was chosen for this project, taking into account economy, the complexity of control, simplicity of construction and energy efficiency [40].

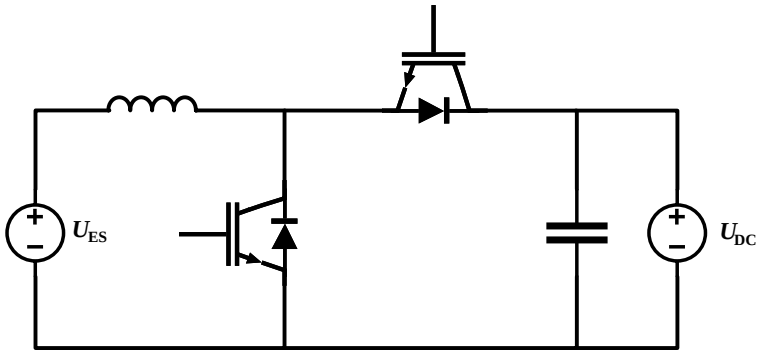

Figure 2.8: Schematic of the Half-bridge Bi-directional DC-DC Converter

As shown in Figure 2.8, the half-bridge bi-directional DC-DC converter has the simplest structure, and the switching device is less stressed in terms of voltage and current in various operating modes.

2.2.2 Operating Principle of Bi-directional DC-DC Converter

This project implies that the port voltages of both the SC arrays and the lithium-ion BAT arrays are lower than the DC link voltage of the ADA under all operating conditions.

$$U_{\mathrm{DC}} > U_{\mathrm{ES}} \tag{2.24}$$

Therefore, by distinguishing the operating power demands of the HESS, the bi-directional DC-DC converter on the HESS can be classified into the following three operating conditions.

Boost Condition

Under Boost conditions, energy is expected to be transferred from the HESS to the DC link of the ADA. Such a DC-DC converter can be equated to the circuit shown in Figure 2.9(a). In one cycle of switching control, this converter can, in turn, be considered as two equivalent circuits as shown in Figure 2.9(b)(c).

When the switching device is in the on state, there are two loops in the entire circuit, and according to Kirchhoff's voltage law, Figure 2.9(b) can be described as follows.

$$U_{\mathrm{ES}} = L\frac{\mathrm{d}i_L}{\mathrm{d}t} = L\frac{\Delta i_{\mathrm{on}}}{T_{\mathrm{on}}} \tag{2.25}$$

$$U_{\mathrm{DC}} = U_C \tag{2.26}$$

When the switching device is in the off state, accordingly, it is also obtained that

$$U_{\mathrm{ES}} = L\frac{\mathrm{d}i_L}{\mathrm{d}t} + U_{\mathrm{DC}} = L\frac{\Delta i_{\mathrm{off}}}{T_{\mathrm{off}}} + U_{\mathrm{DC}} \tag{2.27}$$

where $\Delta i_{\mathrm{on/off}}$ is the variation of inductor current at corresponding state, $T_{\mathrm{on/off}}$ is the time interval of corresponding state.

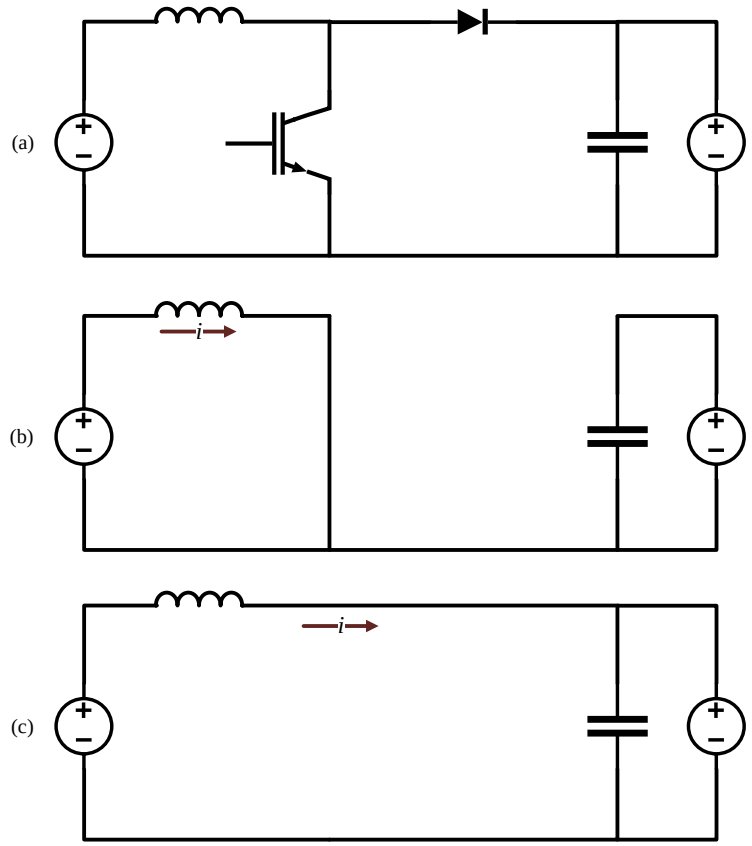

Figure 2.9: Equivalent Circuit of the DC-DC Converter under Boost Condition

At steady state, these gives $\Delta i_{\text{on}} > 0$, $\Delta i_{\text{off}} < 0$ and $\Delta i_{\text{on}} + \Delta i_{\text{off}} = 0$, so that the voltages of two sides defined as:

$$U_{\text{DC}} = \frac{U_{\text{ES}}}{1 - D} \quad (0 \leq D < 1) \tag{2.28}$$

where the duty cycle of the switching signal D is defined as $\frac{T_{\text{on}}}{T_{\text{on}}+T_{\text{off}}}$.

Buck Condition

Under Buck condition, energy is demanded to be transferred from the DC link of the ADA to the HESS. Such a DC-DC converter can be equated to the circuit shown in Figure 2.10(a). In one cycle of switching control, this converter can be recognised as two equivalent circuits as manifested in Figure 2.10(b)(c).

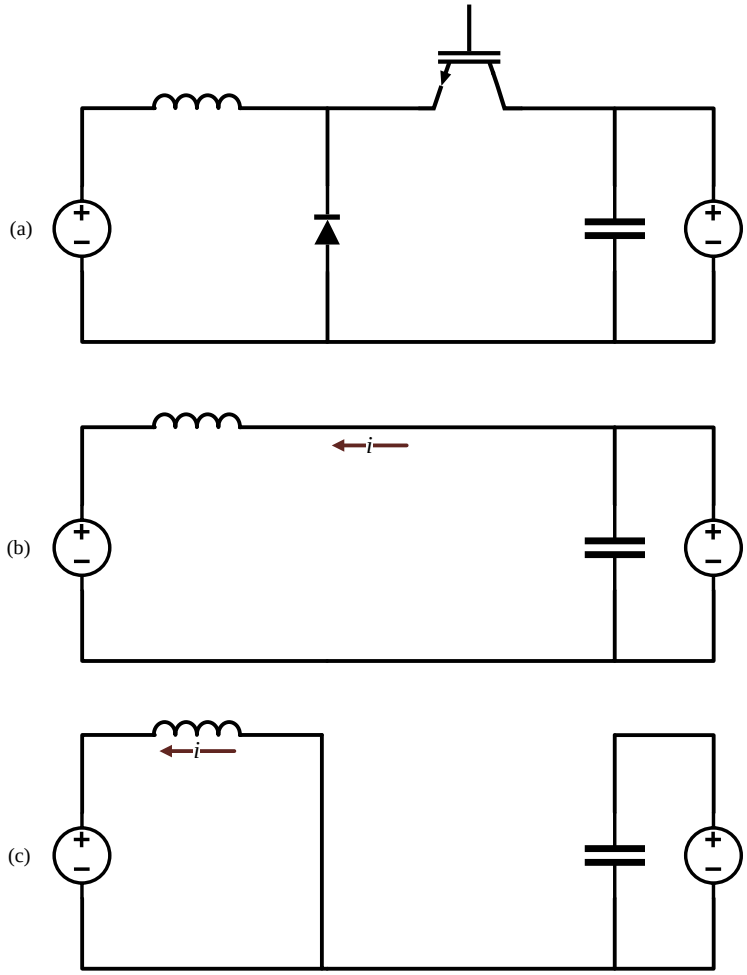

Figure 2.10: Equivalent Circuit of the DC-DC Converter under Buck Condition

When the switching device is in the on state, there is one loop in the complete circuit, and according to Kirchhoff's voltage law, Figure 2.10(b) can be described as follows.

$$U_{\mathrm{ES}} = L\frac{\mathrm{d}i_L}{\mathrm{d}t} + U_{\mathrm{DC}} = L\frac{\Delta i_{\mathrm{on}}}{T_{\mathrm{on}}} + U_{\mathrm{DC}} \tag{2.29}$$

When the switching device is in the off state, accordingly, it is also obtained that

$$U_{\mathrm{ES}} = L\frac{\mathrm{d}i_L}{\mathrm{d}t} = L\frac{\Delta i_{\mathrm{off}}}{T_{\mathrm{off}}} \tag{2.30}$$

$$U_{\mathrm{DC}} = U_C \tag{2.31}$$

where $\Delta i_{\mathrm{on/off}}$ is the variation of inductor current at corresponding state, $T_{\mathrm{on/off}}$ is the time interval of corresponding state.

At steady state, these gives $\Delta i_{\mathrm{on}} < 0$, $\Delta i_{\mathrm{off}} > 0$ and $\Delta i_{\mathrm{on}} + \Delta i_{\mathrm{off}} = 0$, so that the voltages of two sides defined as:

$$U_{\mathrm{ES}} = DU_{\mathrm{DC}} \quad (0 < D \leq 1) \tag{2.32}$$

where the duty cycle of the switching signal D is defined as $\frac{T_{\mathrm{on}}}{T_{\mathrm{on}}+T_{\mathrm{off}}}$.

Inactivity Condition

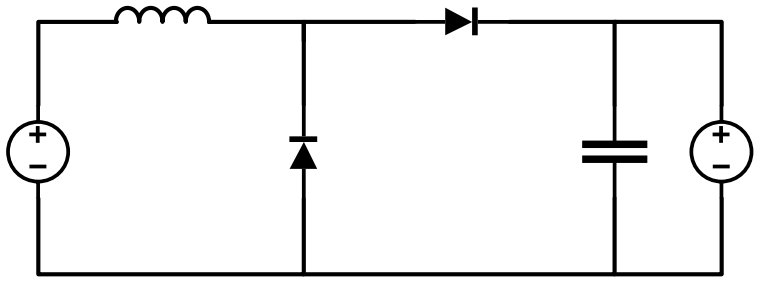

Figure 2.11: Equivalent Circuit of the DC-DC Converter under Inactivity Condition

In this condition, the converter blocks the bilateral energy flow. Therefore, the converter can be equated to the circuit displayed in Figure 2.11. This mode is essential to maintain the proper operation of the HESS and to prolong its lifetime.

2.3 Complete Topology of HESCPSS

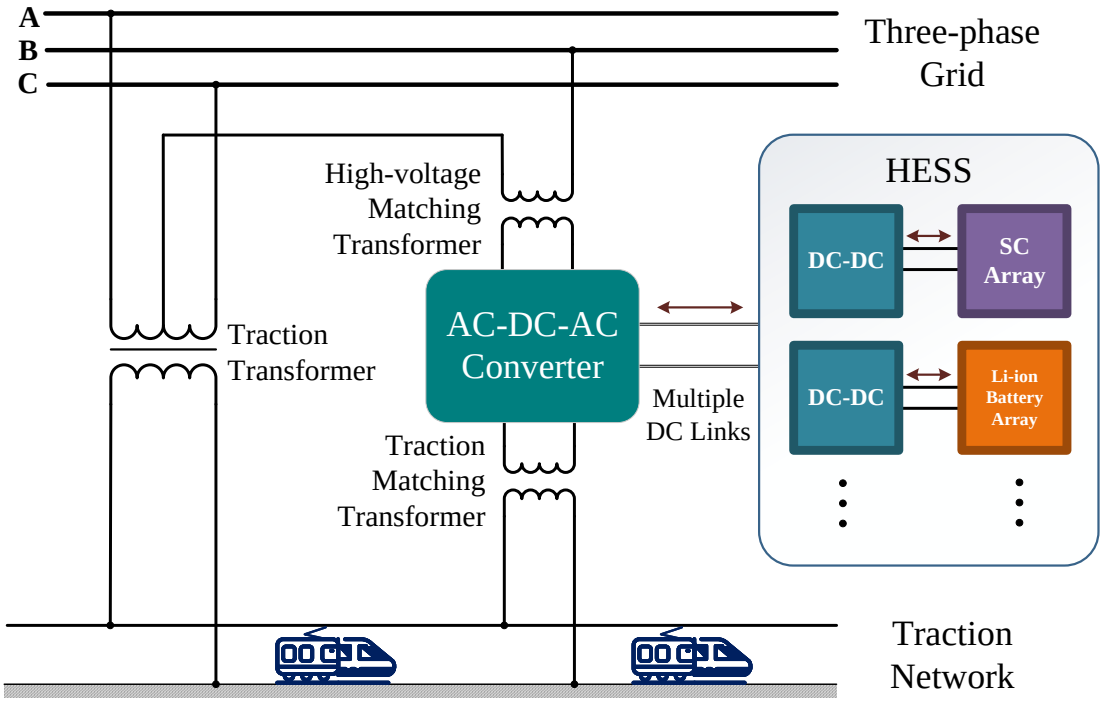

Figure 2.12: Complete Structure of Proposed HESCPSS

Combining all the elements discussed in this chapter leads to a complete topology on HESCPSS, shown in Figure 2.12. Overall, the proposed topology has the following advances.

1. For three-phase grids, this system, complemented by suitable control methods, is well placed to achieve very high power quality, with negative sequence currents and harmonics adequately mitigated.
2. Both TT and CPD can flexibly cope with positive and negative power, making the utilisation of RBE feasible. Further, the DC link in the ADA can also flexibly interact with the HESS, which can greatly enhance the utilisation of the RBE.
3. The introduction of the HESS allows for adaptable adjustment of the power demand on the grid side and, through appropriate control methods, can reduce the demand on the grid by storing energy in the HESS during load power troughs and releasing energy from the HESS during load power surges.
4. The application of combined CTPSS, cascaded H-bridge ADA, and half-bridge DC-DC converters result in a sound balance of overall system cost and performance.

In the next chapter, each of the HESCPSS operating patterns will be discussed separately.

Chapter 3

Operating Patterns of Hybrid Energy Storage Co-phase Power Supply System

In this chapter, different HESCPSS operating patterns can be obtained by classifying the varying load power levels. Consequently, the characteristics and the desired energy flow patterns are analysed separately.

3.1 Traction Power Flow Conditions

The operating patterns of the HESCPSS can be divided into three types for different traction load power levels.

- Demand Trough Smoothing Patterns (TR)
- Demand Surge Smoothing Patterns (SG)
- Regenerative Braking Patterns (RB)

These types have distinct power properties, and by distinguishing between them, the objectives of energy utilisation in the overall system vary, power quality including three-phase voltage unbalance and HESS lifetime can be well balanced.

It is important to note that in the analysis in this section, the following assumptions are considered.

1. The locomotives used in modern HSR, especially the AC/DC/AC type, have a power factor close to 1 and excellent reactive power and harmonic performance. Therefore the load power discussed in this section carries only active power P_L [4], i.e. the traction load is considered a purely resistive load.
2. It is assumed that, for positive load values ($P_L > 0$), the load is powered by the system; for negative load values ($P_L < 0$), the load is in its regenerative braking mode.
3. Assume that the power passing through the TT P_{TT} is positive when energy is transferred from the grid to the traction load, vice versa.
4. Assume that the power passing through the CPD's HMT and α port P_α is positive when energy flows from the grid to the ADA's α port; the power passing through the CPD's TMT and β port P_β is positive when energy flows from the CPD to the traction load; the

power flow from the DC-Link of the ADA to the HESS P_{HESS} is positive when HESS is absorbing energy, hence negative when releasing.

5. Also, for the purpose of analysis, the CPD is considered as a device with no energy loss.

Thus, the following mathematical relationships can be obtained

$$P_L = P_{\mathrm{TT}} + P_\beta \tag{3.1}$$
$$P_\alpha = P_\beta + P_{\mathrm{HESS}} \tag{3.2}$$

3.1.1 Demand Trough Smoothing Patterns

In order to improve the cost-effectiveness of the HESCPSS, the HESS needs to be charged at the appropriate time. The system can be operated in this mode when the traction load power is less than the threshold value P_{TR}. In these patterns, TT supplies the load, while CPD charges the HESS. Charging the HESS when the traction load is low and powering replenishment at summit load circumstances contributes to lower demand power costs on the grid side.

Further, HESS usually has a limit on the charging and discharging power $\overline{P_{\mathrm{HESS}}}$, which is highly relevant to the expense of HESS. Based on this limitation, the pattern can be further split into two patterns as follows, and the corresponding power flow allocations are indicated in Figure 3.1.

(a) Demand Trough Smoothing Pattern 1

When the load power does not reach the HESS power limit ($0 < P_L < \overline{P_{\mathrm{HESS}}}$), in order to fully balance the negative sequence current, according to Equation 2.15, HMT should has identical power flow as the TT . That is

$$\begin{array}{rcl} P_\alpha & = & P_L \\ P_{\mathrm{HESS}} & = & P_L \\ P_\beta & = & 0 \\ P_{\mathrm{TT}} & = & P_L \end{array} \tag{3.3}$$

(b) Demand Trough Smoothing Pattern 2

When the load power exceeded the HESS power limit ($\overline{P_{\mathrm{HESS}}} < P_L < P_{\mathrm{TR}}$), the HESS is charged at the maximum permissible power through the CPD. That is

$$\begin{array}{rcl} P_\alpha & = & \overline{P_{\mathrm{HESS}}} \\ P_{\mathrm{HESS}} & = & \overline{P_{\mathrm{HESS}}} \\ P_\beta & = & 0 \\ P_{\mathrm{TT}} & = & P_L \end{array} \tag{3.4}$$

Then, based on Equation 2.12, the three-phase unbalance factor:

$$\varepsilon_u = \frac{P_L - \overline{P_{\mathrm{HESS}}}}{S_{\mathrm{sc}}} \times 100\% \tag{3.5}$$

which should be limited in a standard range. Thus, the selection of value of the power threshold is vital, and this will be discussed in the next chapter.

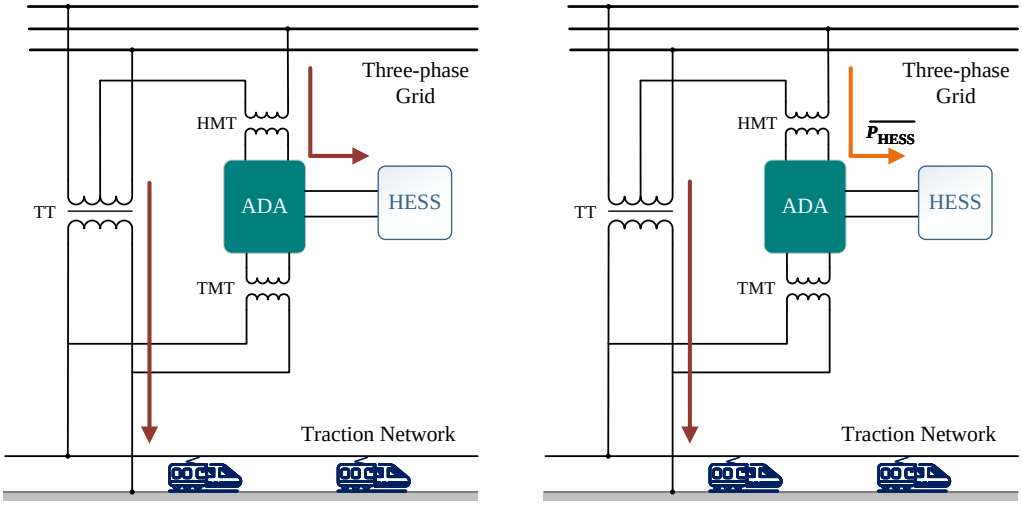

Figure 3.1: Power Flow Allocation of Demand Trough Smoothing Patterns

3.1.2 Demand Surge Smoothing Patterns

The traction load has a high dynamic range and, in particular, a very high peak traction power. The CPD introduced by the combined CTPSS can share the traction load with the TT , and together with the introduction of the HESS, the overall system can be relieved of the burden when large surges in traction load occur.

In order to minimise the number of charge/discharge cycles of the HESS while meeting the power quality requirements, this pattern can be subdivided into two distinct patterns depending on the power level of the traction load. The boundary threshold between these two patterns is defined as P_{SG}.

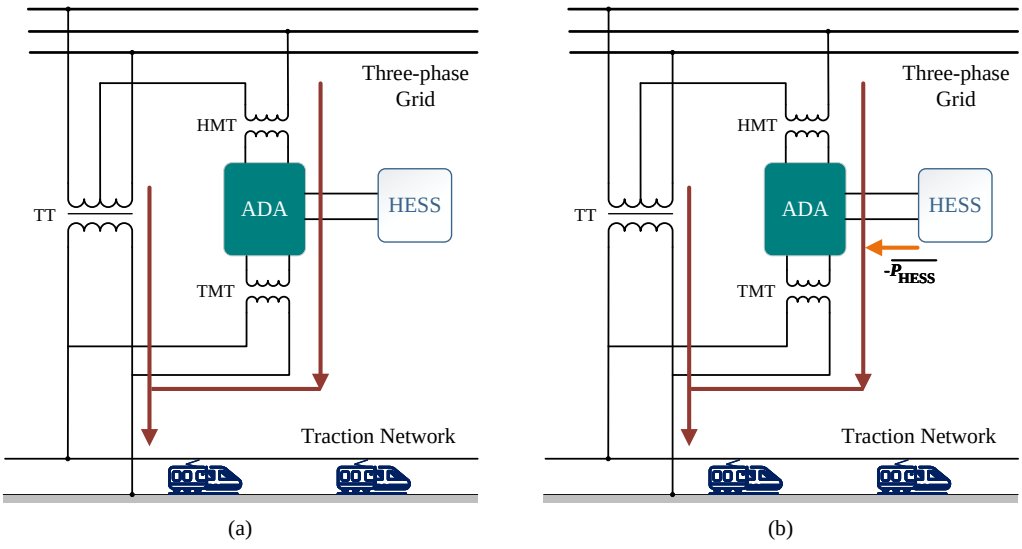

Figure 3.2: Power Flow Allocation of Demand Surge Smoothing Patterns

(a) Demand Surge Smoothing Pattern 1

When the load power does not reach the Surge threshold ($P_{\mathrm{TR}} < P_L < P_{\mathrm{SG}}$), the load is supplied by TT and CPD while HESS is inactive. The CPD conditions:

$$\begin{array}{rcc} P_\alpha & = & P_L - P_{\mathrm{TT}} \\ P_{\mathrm{HESS}} & = & 0 \\ P_\beta & = & P_L - P_{\mathrm{TT}} \end{array} \tag{3.6}$$

According to Equation 2.15,

$$P_{\mathrm{TT}} = \frac{\varepsilon_u \times S_{\mathrm{sc}}}{2} + \frac{P_L}{2} \tag{3.7}$$

$$P_\alpha = -\frac{\varepsilon_u \times S_{\mathrm{sc}}}{2} + \frac{P_L}{2} \tag{3.8}$$

Linking Equations 3.6-3.8, one can obtain the CPD power flow conditions:

$$P_\alpha = P_\beta = -\frac{\varepsilon_u \times S_{\mathrm{sc}}}{2} + \frac{P_L}{2} \tag{3.9}$$

$$P_{\mathrm{HESS}} = 0 \tag{3.10}$$

(b) Demand Surge Smoothing Pattern 2

When the load power exceeds the Surge threshold ($P_{\mathrm{SG}} < P_L$), the load is supplied by TT and CPD while HESS is discharging at its maximum power. The CPD conditions:

$$\begin{array}{rcc} P_\alpha & = & P_L - P_{\mathrm{TT}} - P_{\mathrm{HESS}} \\ P_{\mathrm{HESS}} & = & -\overline{P_{\mathrm{HESS}}} \\ P_\beta & = & P_L - P_{\mathrm{TT}} \end{array} \tag{3.11}$$

According to Equation 2.15,

$$P_{\mathrm{TT}} = \frac{\varepsilon_u \times S_{\mathrm{sc}}}{2} + \frac{P_L - \overline{P_{\mathrm{HESS}}}}{2} \tag{3.12}$$

$$P_\alpha = -\frac{\varepsilon_u \times S_{\mathrm{sc}}}{2} + \frac{P_L - \overline{P_{\mathrm{HESS}}}}{2} \tag{3.13}$$

Linking Equations 3.11-3.13, one can obtain the CPD power flow conditions:

$$P_\alpha = -\frac{\varepsilon_u \times S_{\mathrm{sc}}}{2} + \frac{P_L - \overline{P_{\mathrm{HESS}}}}{2} \tag{3.14}$$

$$P_\beta = -\frac{\varepsilon_u \times S_{\mathrm{sc}}}{2} + \frac{P_L + \overline{P_{\mathrm{HESS}}}}{2} \tag{3.15}$$

$$P_{\mathrm{HESS}} = -\overline{P_{\mathrm{HESS}}} \tag{3.16}$$

3.1.3 Regenerative Braking Patterns

RBE from locomotives is fed directly back into the grid or consumed via a mechanical or electrical load in conventional systems, which wastes vast amounts of energy and is also likely to have a negative impact on the power quality of the grid. HESCPSS can take full advantage

of its elastic energy flow to improve the utilisation of the RBE and further improve the overall system economy.

Because of the introduction of the HESS, priority can be given to collecting the RBE into the HESS rather than returning it to the grid via the TT . Based on such a principle, the different RBE power levels can be divided into several patterns for discussion.

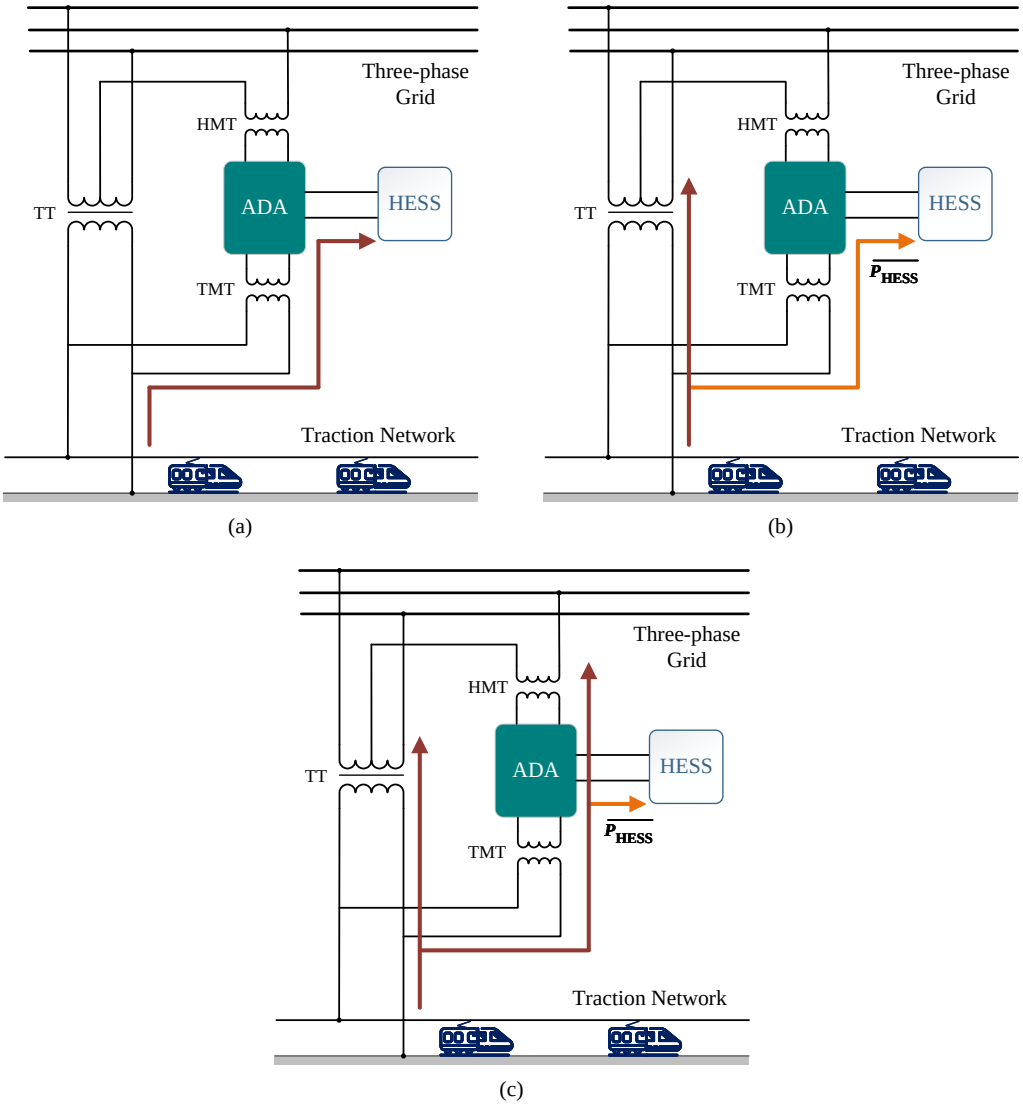

Figure 3.3: Power Flow Allocation of Regenerative Braking Patterns

(a) Regenerative Braking Pattern 1

When the power of the RBE generated by the locomotive does not surpass the HESS power limit ($-\overline{P_{\text{HESS}}} < P_L < 0$), all of the RBE is charged to the HESS via the β phase interface of the CPD. Therefore, the CPD conditions:

$$\begin{aligned} P_\alpha &= 0 \\ P_{\text{HESS}} &= -P_L \\ P_\beta &= P_L \end{aligned} \tag{3.17}$$

Note that no power is intended to flow into the grid in this pattern, hence no influence on the power quality of the three-phase grid.

(b) Regenerative Braking Pattern 2

When the power of the RBE generated by the locomotive exceeds the maximum charge power limit of the HESS but does not exceed a preset threshold ($P_{\mathrm{RB}} < P_L < -\overline{P_{\mathrm{HESS}}}$), the HESS absorbs a portion of the RBE at maximum power via the β phase interface of the CPD and the remainder is fed back into the grid by the TT . Therefore, the CPD conditions:

$$\begin{array}{rcc} P_\alpha & = & 0 \\ P_{\mathrm{HESS}} & = & \overline{P_{\mathrm{HESS}}} \\ P_\beta & = & -\overline{P_{\mathrm{HESS}}} \end{array} \tag{3.18}$$

Consequently, the power through TT is

$$P_{\mathrm{TT}} = P_L - P_\beta = P_L - (-\overline{P_{\mathrm{HESS}}}) \tag{3.19}$$

Then, based on Equation 2.12, the three-phase unbalance factor under this pattern:

$$\varepsilon_u = \frac{P_L + \overline{P_{\mathrm{HESS}}}}{S_{\mathrm{sc}}} \times 100\% \tag{3.20}$$

(c) Regenerative Braking Pattern 3

When the power of the RBE generated by the locomotive exceeds a set threshold ($P_L < P_{\mathrm{RB}}$), the RBE is fed back to the grid simultaneously by the TT and the CPD while passing into a part of the CPD to charge the HESS at its maximum power. Thus, the following power flow conditions about CPD:

$$\begin{array}{rcc} P_\alpha & = & P_L + \overline{P_{\mathrm{HESS}}} - P_{\mathrm{TT}} \\ P_{\mathrm{HESS}} & = & \overline{P_{\mathrm{HESS}}} \\ P_\beta & = & P_L - P_{\mathrm{TT}} \end{array} \tag{3.21}$$

According to Equation 2.15,

$$P_{\mathrm{TT}} = \frac{\varepsilon_u \times S_{\mathrm{sc}}}{2} + \frac{P_L + \overline{P_{\mathrm{HESS}}}}{2} \tag{3.22}$$

$$P_\alpha = -\frac{\varepsilon_u \times S_{\mathrm{sc}}}{2} + \frac{P_L + \overline{P_{\mathrm{HESS}}}}{2} \tag{3.23}$$

Linking Equations 3.21-3.23, one can obtain the CPD power flow conditions:

$$P_\alpha = -\frac{\varepsilon_u \times S_{\mathrm{sc}}}{2} + \frac{P_L + \overline{P_{\mathrm{HESS}}}}{2} \tag{3.24}$$

$$P_\beta = -\frac{\varepsilon_u \times S_{\mathrm{sc}}}{2} + \frac{P_L - \overline{P_{\mathrm{HESS}}}}{2} \tag{3.25}$$

$$P_{\mathrm{HESS}} = \overline{P_{\mathrm{HESS}}} \tag{3.26}$$

3.2 Summary of Patterns

Based on patterns discussed in this chapter, a comparative table of the quantity of power across all ports of the HESCPSS can be summarised, as shown in Table 3.1.

Table 3.1: Comparison of HESCPSS Operating Patterns

Pattern	P_L Lower Limit	P_{TT}	P_α	P_{HESS}
RB (c)	-	$\frac{1}{2}(\varepsilon_u S_{\mathrm{sc}} + P_L + \overline{P_{\mathrm{HESS}}})$	$\frac{1}{2}(-\varepsilon_u S_{\mathrm{sc}} + P_L + \overline{P_{\mathrm{HESS}}})$	$\overline{P_{\mathrm{HESS}}}$
RB (b)	P_{RB}	$P_L + \overline{P_{\mathrm{HESS}}}$	0	$\overline{P_{\mathrm{HESS}}}$
RB (a)	$-\overline{P_{\mathrm{HESS}}}$	0	0	$-P_L$
TR (a)	0	P_L	P_L	P_L
TR (b)	$\overline{P_{\mathrm{HESS}}}$	P_L	$\overline{P_{\mathrm{HESS}}}$	$\overline{P_{\mathrm{HESS}}}$
SG (a)	P_{TR}	$\frac{1}{2}(\varepsilon_u S_{\mathrm{sc}} + P_L)$	$\frac{1}{2}(-\varepsilon_u S_{\mathrm{sc}} + P_L)$	0
SG (b)	P_{SG}	$\frac{1}{2}(\varepsilon_u S_{\mathrm{sc}} + P_L - \overline{P_{\mathrm{HESS}}})$	$\frac{1}{2}(-\varepsilon_u S_{\mathrm{sc}} + P_L - \overline{P_{\mathrm{HESS}}})$	$-\overline{P_{\mathrm{HESS}}}$

where ε_u is the three-phase unbalance factor, which is usually a predetermined target. And that the power of β port is always regulated as $P_\beta = P_\alpha - P_{\mathrm{HESS}}$.

As can be found from Table 3.1, each operating patterns correspond to an individual P_L value interval, and these intervals do not intersect with each other, i.e. a unique operating mode can be undoubtedly determined by P_L. This implies constraints about these threshold that $P_{\mathrm{RB}} < -\overline{P_{\mathrm{HESS}}} < 0 < \overline{P_{\mathrm{HESS}}} < P_{\mathrm{TR}} < P_{\mathrm{SG}}$. It is also manifest from the table that most of the power targets vary according to the P_L and that this variation can also be considered almost continuous between patterns. Thus, the operating patterns model, designed as above, can significantly facilitate the design of control methods for this project, which will be discussed in the next section.

Chapter 4

Control Strategy of Hybrid Energy Storage Co-phase Power Supply System

This chapter will discuss the control methods for each part of the HESCPSS individually, and this includes the methods for generating the specific gate-level signals for the power electronic converters and the methods for accurately controlling the power flow. A higher-level control strategy for integrating the system will also be discussed, which recognises the economics under multiple scenarios. The result is a practical two-level control strategy.

4.1 Lower Level Control

In the lower level of control, the reference power values of each electrical port are passed in, then data such as the port reference voltage and reference current are calculated by the controllers. Based on these data, PWM modulated switching signals, which can be used to drive the power switching devices of the power electronics converters in the combined CTPSS and HESS, are generated. These switching signals are expected to achieve the desired power transfer, allowing the corresponding converter to operate in the specified operating condition.

4.1.1 Control of AC-DC-AC Converter

In the previous chapters, a clear conclusion can be drawn that for the control of combined CTPSS, the key lies in controlling the converter in the ADA. With the proper control manoeuvres, it is possible to compensate as much as possible for reactive power and harmonics on both sides of the ports. By distinguishing whether the current on the AC side is included in the calculation sequences of the controllers, the control methods of the ADA can be divided into indirect and direct current control [41]. Although indirect current control has the strengths of low cost and low practical engineering difficulty, its performance on tracking the AC-side current is limited compared to the direct current control method, with the inadequate dynamic response of the overall system and poor steady-state results. Therefore, only direct current control methods are addressed in this project.

The Figure 4.1 is the block diagram of the calculation sequence for the controller of the ADA used in this project. It is not surprising that, similar to the previous topology where ADA was considered symmetrical and independent, the ADA control method also practices symmetri-

cal and independent computational sequence. Therefore, when interpreting and analysing the algorithm, this subsection discusses the control of the α phase side only.

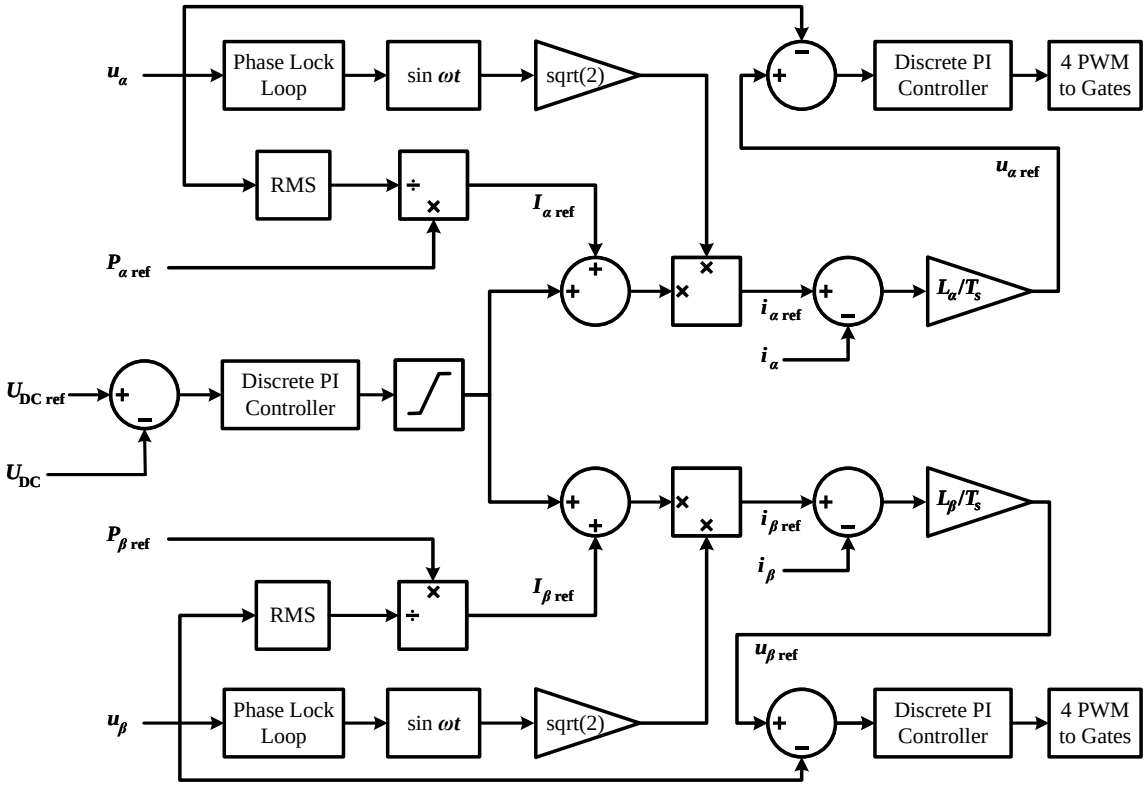

Figure 4.1: Control Method of ADA in Combined CTPSS

Firstly, for the control method discussed in this subsection, here are the electrical quantities to be collected:

1. u_α, i_α: the instantaneous voltage and current of port α.
2. u_β, i_β: the instantaneous voltage and current of port β.
3. U_{DC}: the voltage of the DC link.

It is also necessary to assume the reference powers of two ports $P_{\alpha\mathrm{ref}}, P_{\beta\mathrm{ref}}$ derived from the upper layer control. The final output of this control method is the gate-level Boolean signals of the individual power switching devices of the converter. The following is a comprehensive description of the calculation process.

Starting from the outermost layer, the voltage on the DC link U_{DC} is first sampled and then compared with the reference voltage of the DC link U_{DCref} to produce a DC regulating control component via a discrete PI controller with a limiter. On the α phase side of this converter, the component regarding the RMS value of the port current is calculated by dividing the given reference active power $P_{\alpha\mathrm{ref}}$ by the RMS value of the sampled α port voltage u_α.

The two components presently calculated are summed, and their sum is considered as the RMS value of α port reference current $I_{\alpha\mathrm{ref}}$. At the same time, the phase information of the port

voltage u_α is obtained through the phase-locked loop and the corresponding sinusoidal function value is generated, which is amplified by $\sqrt{2}$ and multiplied by the RMS value of the port reference current $I_{\alpha\mathrm{ref}}$ to obtain the reference of instantaneous port current $i_{\alpha\mathrm{ref}}$.

Considering the traditional current control process of the converter, the current sampling period and the delay of the control signal can have an impact on the dynamic performance of the current tracking. Therefore, in this project, the predictive current control with overrun characteristics is applied to the ADA's control to weaken the adverse effects caused by the control delay to a certain extent to achieve a better dynamic compensation outcome [42].

Firstly, assume that the controller samples the current and voltage information of the converter at a fixed period T_s, and that both the calculation period of the controller and the modulation period of the PWM are also T_s. Predictive current control means that the actual current value at the current sampling moment $i_\alpha(t = \tau)$ is compared with the reference value of the predicted current at the subsequent sampling period $i_{\alpha\mathrm{ref}}(t = \tau + T_s)$, then the control voltage is calculated. Depending on the nature of the current through the AC side inductor L_α, the actual current value at the next sampling period is forced to tail after the reference current value at the next sampling period, i.e. always trying to be slightly advanced of the present situation. Assuming that the current sampling time is τ, current tracking in effect, in steady-state, the relationship between the actual current and the reference current in following one sampling period can be expressed as:

$$i_\alpha(t = \tau + T_s) = i_{\alpha\mathrm{ref}}(t = \tau) \tag{4.1}$$

The single-phase converter structured in Figure 2.2 is used as an example to analyse the predictive current control of combined CTPSS. According to its equivalent circuit (Figure 2.5), combined with Kirchhoff's voltage law, one obtains:

$$u_\alpha = L_\alpha \frac{\mathrm{d}i_\alpha}{\mathrm{d}t} + u_{\alpha\mathrm{C}} \tag{4.2}$$

where the resistance is much smaller than the reactance of the inductor ($R_\alpha \ll \omega L_\alpha$), the effect of resistance is ignored in the analysis in this subsection. If T_s is sufficiently small and the system is at steady state, it is easy to argue that some quantity can be considered as a constant rather than a function of time. That is, under ideal conditions, it is possible to obtain:

$$u_{\alpha\mathrm{Cref}} = u_\alpha - L_\alpha \frac{\Delta i_\alpha}{T_s} = u_\alpha - L_\alpha \frac{i_\alpha(\tau + T_s) - i_\alpha(\tau)}{T_s} \tag{4.3}$$

Linking this with Equation 4.1:

$$u_{\alpha\mathrm{Cref}} = u_\alpha - L_\alpha \frac{i_{\alpha\mathrm{ref}}(\tau) - i_\alpha(\tau)}{T_s} \tag{4.4}$$

From this equation, it can be seen that the amount of change in inductor current over a sampling period can be equated with the difference between the reference and actual values of the converter current and can be directly related to the inductor voltage. This property allows the instantaneous reference current $i_{\alpha\mathrm{ref}}$ to be applied to find the instantaneous reference voltage of the H-bridge equivalent of the circuit, which is also the instantaneous reference voltage of the controlled voltage source $u_{\alpha\mathrm{Cref}}$.

4.1.2 Control of DC-DC Controller in HESS

In the previous chapters, the structure of the HESS was illuminated. A working units of the HESS consists of two energy storage medium arrays (Li-ion BAT and SC) and corresponding bi-directional DC-DC converters. The Li-ion BAT array and the SC array are attached to the ADA's DC link via a bi-directional DC-DC converter, which controls the absorption and release of energy by controlling the operation mode of the converter. Thus, the pivotal point for controlling the HESS resides in the control of the converters. Besides, the operating modes of this converter have been discussed and analysed individually. In this subsection, the specific control methods regarding the bi-directional DC-DC converter, including the signalling of the power switching devices and the mode switching, will be described.

Firstly, for the control method discussed in this subsection, here are the electrical quantities to be captured:

1. U_{ES}: the voltage of the energy storage device array.
2. I_{ES}: the current of the energy storage device array.
3. $\mathrm{SOC}_{\mathrm{ES}}$: the State-of-charge reported by the energy storage device array.

It is also required to assume the reference powers of this energy storage unit P_{ESref} derived from the higher layer control. The final output of this control method is the gate-level Boolean signals of the individual power switching devices of the converter. The following is a thorough description of the calculation process.

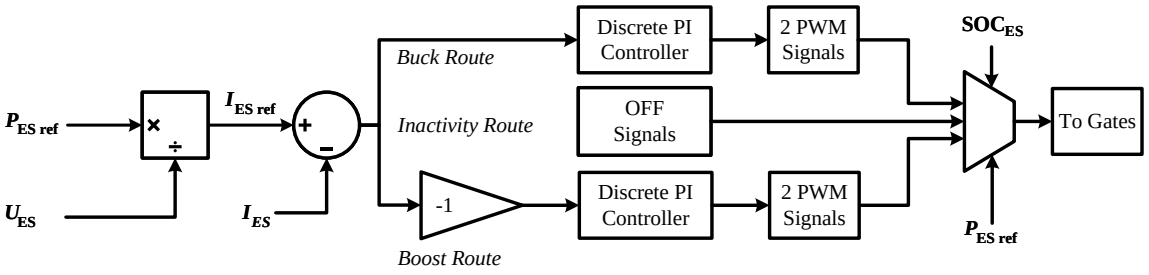

Figure 4.2: Control Method of Converter in HESS

For the control of the bi-directional DC-DC converter, a dual-loop control method with an outer loop of power and an inner loop of current is employed. Firstly, a reference power value P_{ESref} can be obtained from the higher-level control, which is then divided by the array voltage U_{ES} to obtain the target current of the energy storage unit I_{ESref}. By subtracting this target current from the actual current sampled in real-time I_{ES}, a current error value can be obtained. This error value is then fed separately to two discrete PI controllers, who control the Buck and Boost modes of this half-bridge bi-directional DC-DC converter, respectively. These two controllers each generate a set of PWM signals for controlling the two power switching devices on the bridge arm. Finally, an additional set of pure shutdown signals for inactivity mode is considered, and the three sets of signals are fed into a multiplexer and then finally output to the switching devices. This mode selector (multiplexer) operates as shown in Figure 4.3.

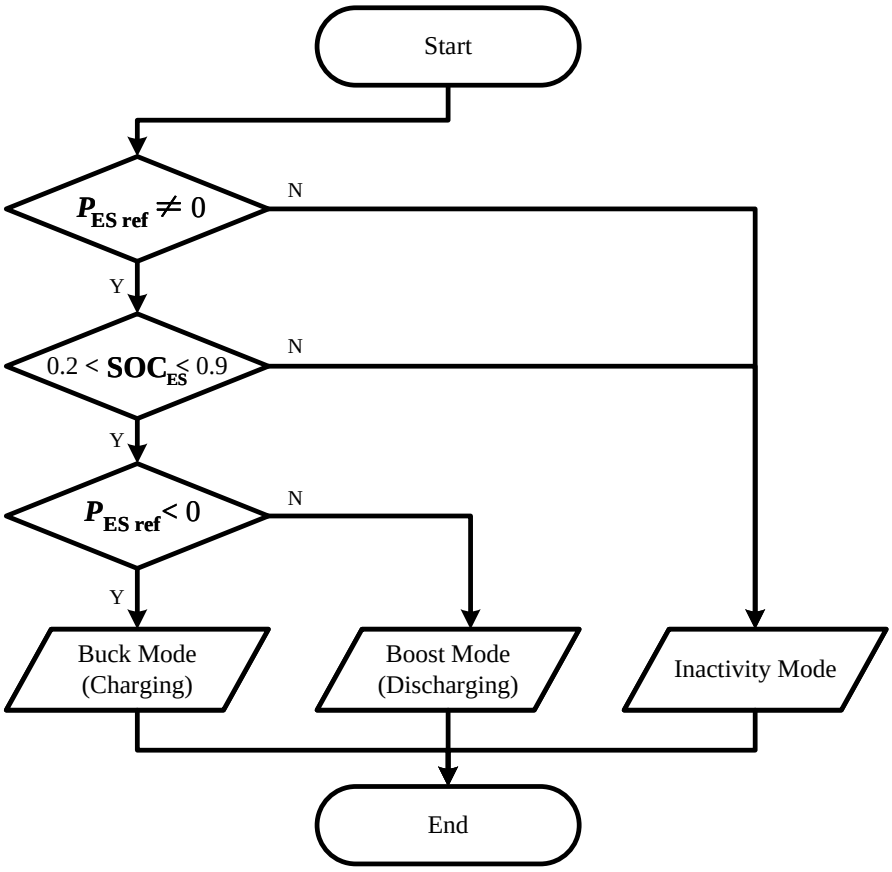

Figure 4.3: Flow Chart of Mode Selector in HESS

This selector first classifies the reference power and then judges the SOC of the energy storage medium array to ensure that it is not over-charged and over-discharged to prolong the overall system lifetime. The judgement shown in the diagram is performed once in each control cycle. This entire control method ensures the proper functioning of the energy storage medium array and flexible mode switching.

4.2 Higher Level Control

After discussing the lower-level control methods for each part of the system, there demands a control layer that works at the higher-level to manage the power flows in the complete HESCPSS. Specifically, this is the generation of all the previously mentioned reference powers by means of some calculation method for the lower-level controllers to complete their control operations.

4.2.1 Power Distribution in HESS

Unlike general ESS, HESS takes the breakthrough point of mixing two or more energy storage mediums to make full use of the superiorities of each type of material to achieve better results. In the HESS, by allocating the real-time charging and discharging power of the Li-ion BAT and

the SC, it is imperative to improve the dynamic response of the system and extend the service life of the energy storage device via a competent distribution method.

The power distribution in HESS needs to consider the respective energy storage characteristics of the energy storage medium. By regarding complementary performance advantages of Li-ion BAT and SC, SC are responsible for storing the high-frequency component of the power to make full use of its advantages of high power density and high-speed response; Li-ion BAT are responsible for storing the low-frequency component of the power, thus reducing the system requirements for the power density of Li-ion BAT, hence to reduce the cycle times of Li-ion BAT arrays as much as possible and extend their service life. The reference power value of the hybrid energy storage pair P_{ESref} is filtered to obtain the low-frequency fluctuation component as the power of the BAT P_{BATref}, and then the remaining part of the low-pass filtered power is adopted as the power of the SC P_{SCref}. For an energy storage unit pair, the energy is distributed in the way shown in Figure 4.4.

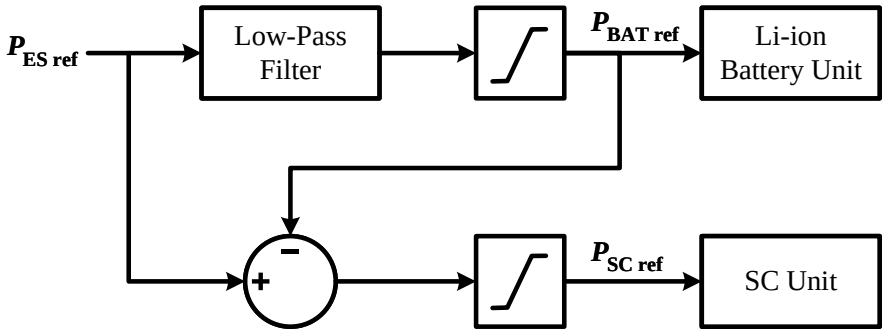

Figure 4.4: Power Distribution Method Applied in HESS

If the effect of the limiters used for protection is not taken into account, the logic of the power distribution can be expressed as:

$$P_{\mathrm{BATref}}(s) = \frac{1}{1 + sT_{\mathrm{LPF}}} P_{\mathrm{ESref}}(s) \tag{4.5}$$

$$P_{\mathrm{SCref}}(s) = \frac{sT_{\mathrm{LPF}}}{1 + sT_{\mathrm{LPF}}} P_{\mathrm{ESref}}(s) \tag{4.6}$$

where s is the complex frequency variables in the Laplacian domain, T_{LPF} is the time constants in low-pass filters. It can be seen that such a power distribution method ensures that the final sum of power allocated to a specific unit is equal to the power reference when all the components do not exceed the limits of the limiter.

4.2.2 Pattern Switching

In addition, the operating patterns discussed in the previous chapters need to be aggregated in this layer to enable flexible switching of individual operating patterns while achieving active power transfer, power quality management, better utilisation of the RBE, optimisation of grid-side electricity demand and many other desired capabilities.

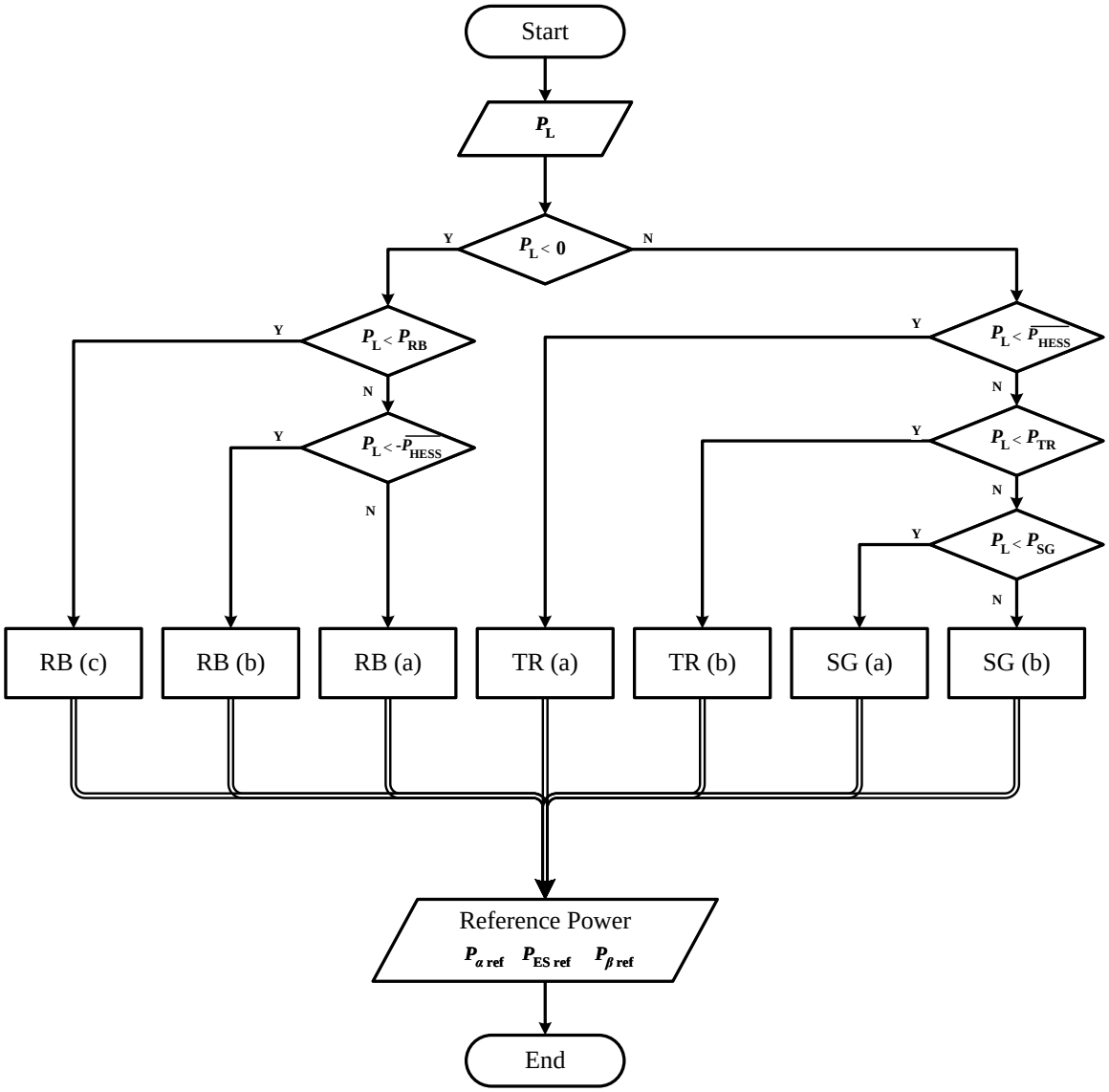

Figure 4.5: Flow Chart of Higher Level Control

Based on the actual requirements, the flow chart shown in Figure 4.5 allows for the allocation of patterns according to the load power level in higher-level control. This high-level control logic can output the reference power of the CPD and HESS to be supplied to the corresponding lower-level controller.

In addition to these logics, the threshold parameters used in the logic need to be determined. Based on the patterns summarised in Figure 3.1, the thresholds for most operating patterns can be set according to the target three-phase unbalance factor. In particular, however, some additional restrictions on RB(b) and TR(b) need to be added.

Take the boundary case for both operating patterns, one can obtain the extreme values of the

three-phase unbalance factor:

$$u_{\mathrm{RB(b)}} = \frac{P_{\mathrm{RB}} + \overline{P_{\mathrm{HESS}}}}{S_{\mathrm{sc}}} < \overline{\varepsilon_u} \tag{4.7}$$

$$u_{\mathrm{TR(b)}} = \frac{P_{\mathrm{TR}} - \overline{P_{\mathrm{HESS}}}}{S_{\mathrm{sc}}} < \overline{\varepsilon_u} \tag{4.8}$$

Consideration of the above relationships ensures that the thresholds are designed to be within the standard limits.

4.3 Overall Control Strategy

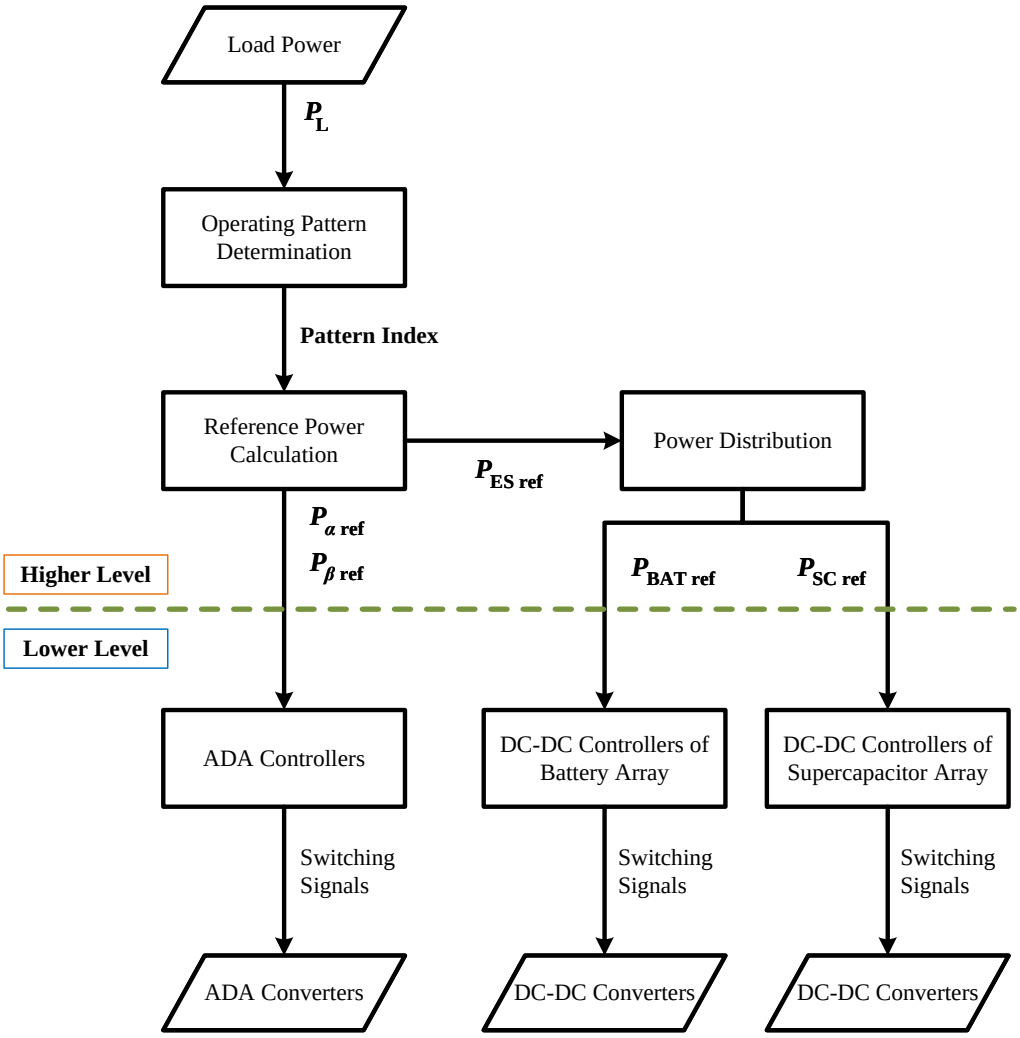

Figure 4.6: Structure of Overall Control Strategy

Based on all the manoeuvres and methodology discussed in this chapter concerning control, a complete control strategy for the system regarding HESCPSS can be derived, as shown in Figure 4.6. The diagram shows the connections between the various control blocks and the information that needs to be communicated between them, as well as the input and output content of the entire control strategy.

Chapter 5

Simulation and Verification

In this chapter, the previously discussed combined CTPSS and HESS will be modelled and simulated. These simulations will be based on MATLAB/Simulink, while the complete logic regarding the control strategy discussed in the previous chapter will also be implemented in MATLAB/Simulink.

First, the overall model of HESCPSS will be verified in MATLAB/Simulink. In sequence, the model's correctness and validity of the combined CTPSS and HESS will be verified to assure that they both work as desired conditions. Then a complete validation of the overall control strategy will be carried out.

As a final step, a case simulation based on actual load power data will be carried out. This case study is based on intra-day data of the power load collected in a traction substation, and the overall effectiveness of the HESCPSS will be verified and analysed.

5.1 MATLAB/Simulink Configuration

5.1.1 Simulation of Combined CTPSS

In MATLAB/Simulink R2021a, a combined CTPSS with the same structure as shown in Figure 2.1 was built. The parameters about this system are synthesized in Table 5.1. The schematics of combined CTPSS and ADA subsystem are demonstrated in Figure 5.1 and Figure 5.2. Note that some of the non-critical measurement interfaces and blocks for exporting data and control have been omitted from the schematics in this chapter to simplify the view.

In contrast to the previously mentioned structures, none of the simulations in this chapter use a multi-stage cascaded H-bridge structure. All cascades have been substituted using their multiplicative equivalent values. As the simulations in this chapter are down to the power switching device and up to the control strategy, and to pursue a quite high simulation accuracy, the system's excessive complexity makes the computer simulation speed extremely limited. With the required number of link stages, i.e. 6 H-bridges and 6 groups of HESS, the simulation is extremely slow, and the space required for RAM is unusually high. Therefore, multiple cascades have been replaced with one equivalent structure. So, firstly the reference voltage on the DC link also becomes $U_{\mathrm{DCref}} = 6 \times 1600\mathrm{V} = 9600\mathrm{V}$. Secondly, therefore, the TMT can be considered as a simple single-phase transformer. Finally, only one set of ADA is retained.

Such a substitution does not affect the model's behaviour but helps to perform a more efficient simulation.

Table 5.1: Parameters Implemented in Simulation of Combined CTPSS

Parameter	Value
Three-phase Grid Voltage	$110\text{kV@}50\text{Hz}$
Short-circuit Capacity S_{sc}	750MVA
Turn Ratio of TT	$(55, 55)/27.5$
Turn Ratio of HMT	$55\sqrt{3}/5.5$
Turn Ratio of TMT	$5.5/27.5$
Inductance of CPD α,β Port L_α, L_β	2mH
Capacitance of CPD DC Link C_{DC}	30mF
Equivalent CPD DC Link Reference Voltage U_{DCref}	9600V

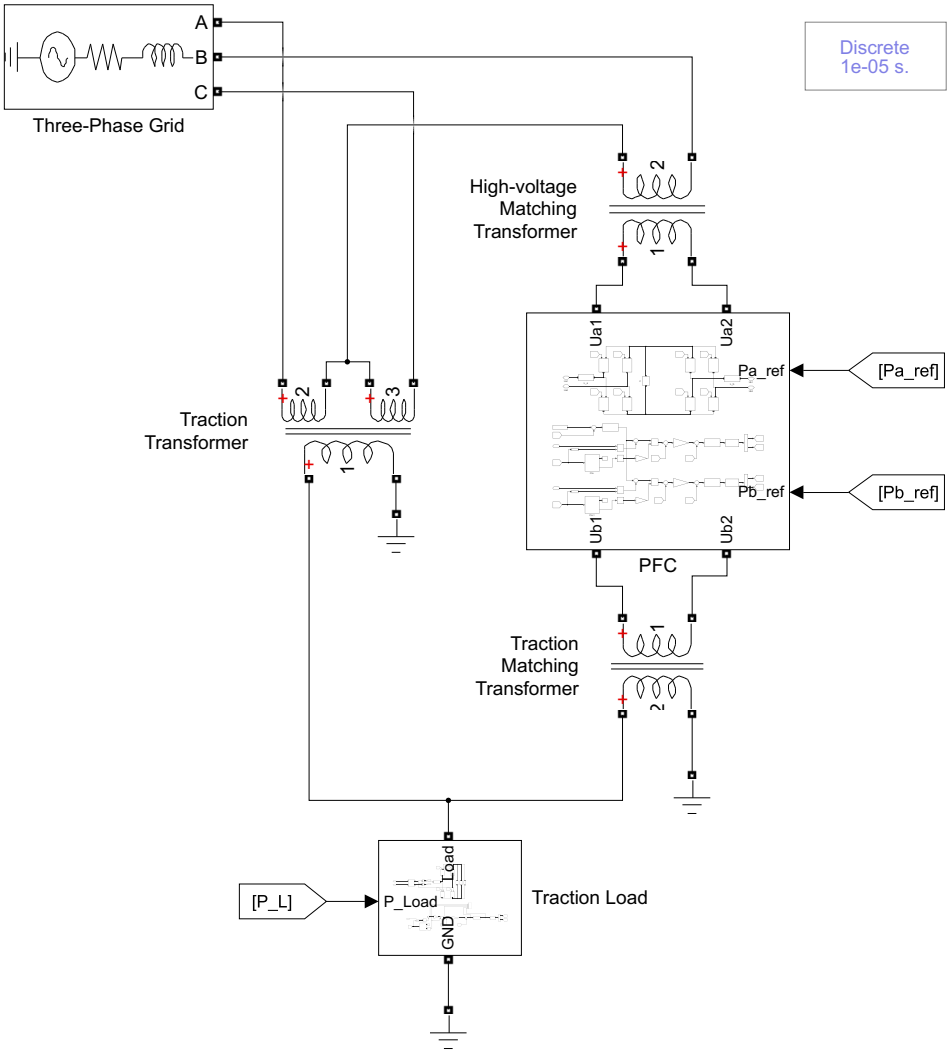

Figure 5.1: Schematic of Combined CTPSS in Simulink

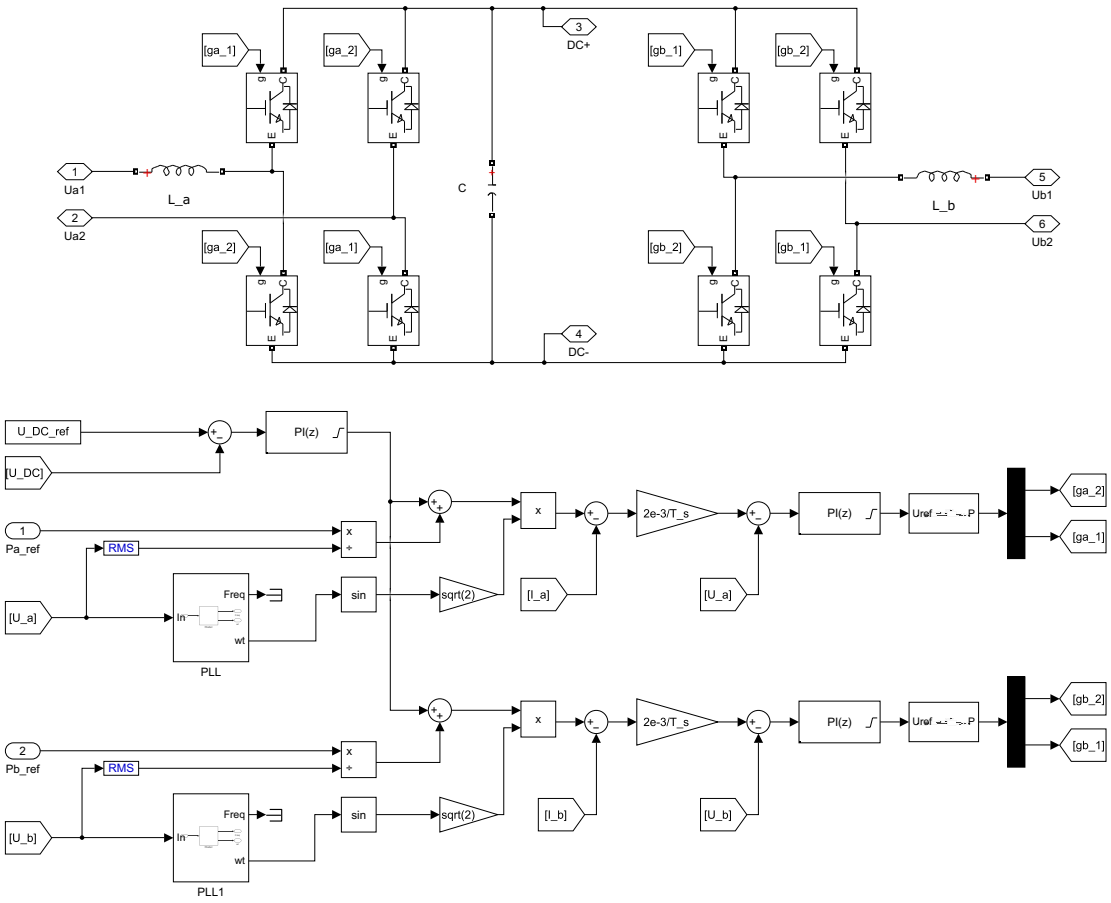

Figure 5.2: Schematic of ADA Subsystem in Simulink

Based on such a simulation model, the following test objectives have been arranged in order to assess the effectiveness of the combined CTPSS.

Table 5.2: Test Objectives for Simulation of Combined CTPSS (0.1s each)

P_L (MW)	CPD Compensate Condition	Expected $P_\alpha = P_\beta$ (MW)
24	No Compensation	0
24	Full Compensation	12
12	Full Compensation	6
-12	Full Compensation	-6

The results of the above tests are presented separately: the active power at each port of the system (Figure 5.3), the three-phase grid-side voltage and current (Figure 5.4), the three-phase unbalance factor derived from the grid-side voltage and current (Figure 5.5), and the voltage at the DC link (Figure 5.6).

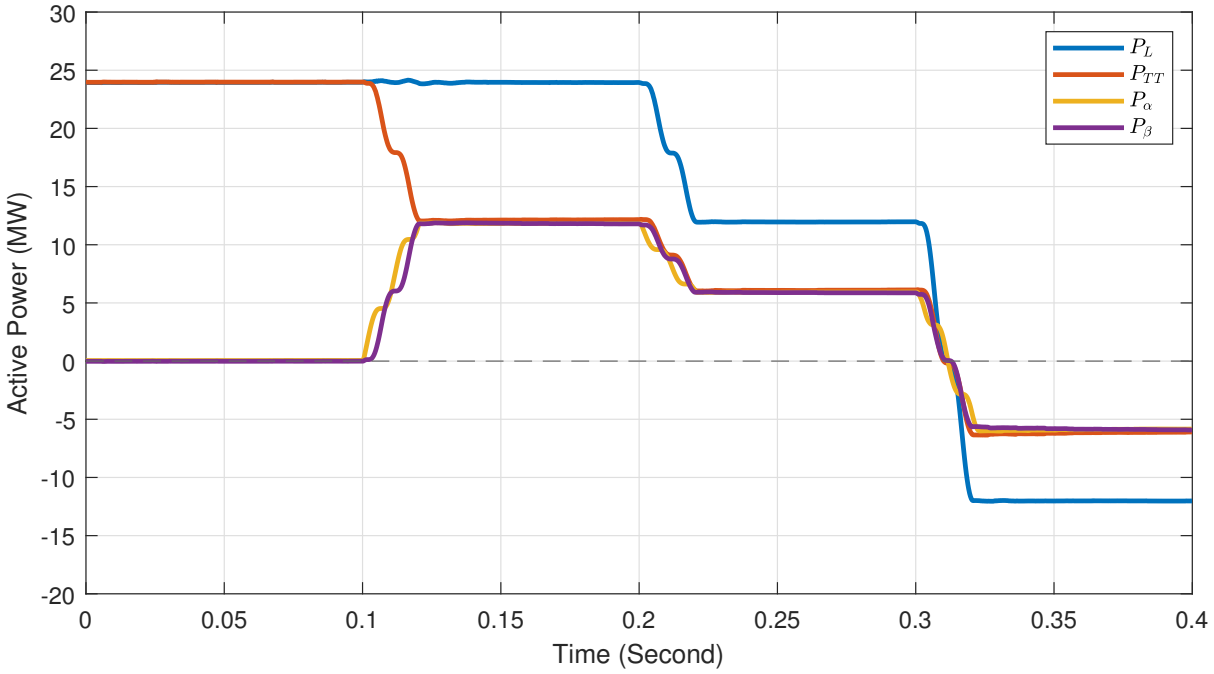

Figure 5.3: Simulation Result: Port Power (Combined CTPSS)

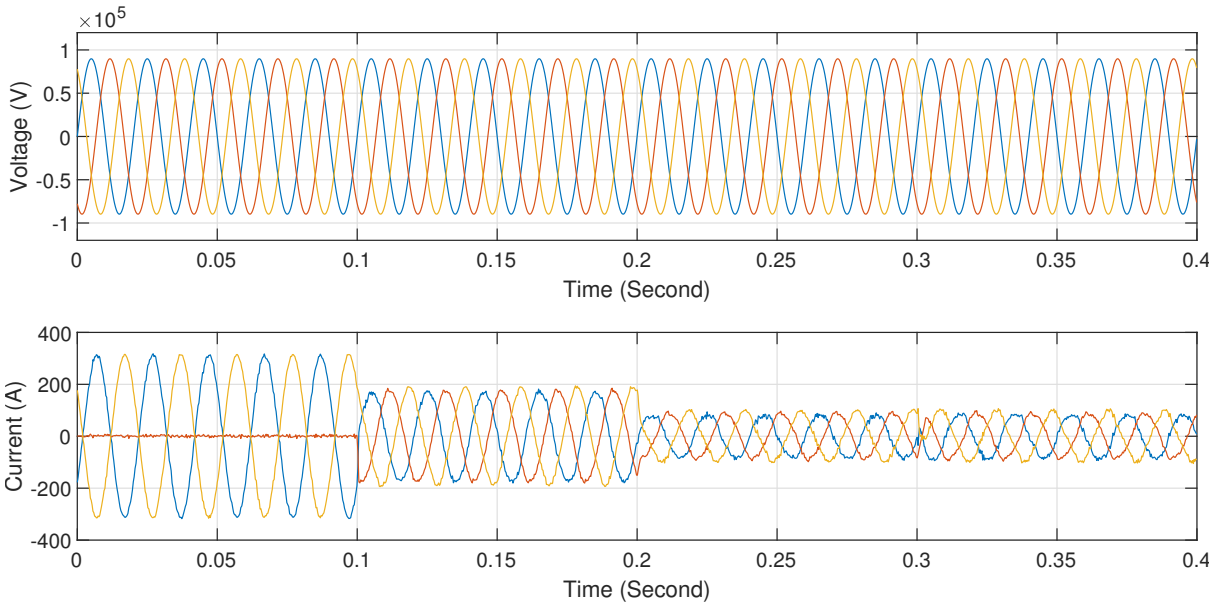

Figure 5.4: Simulation Result: Grid Side Voltage and Current (Combined CTPSS)

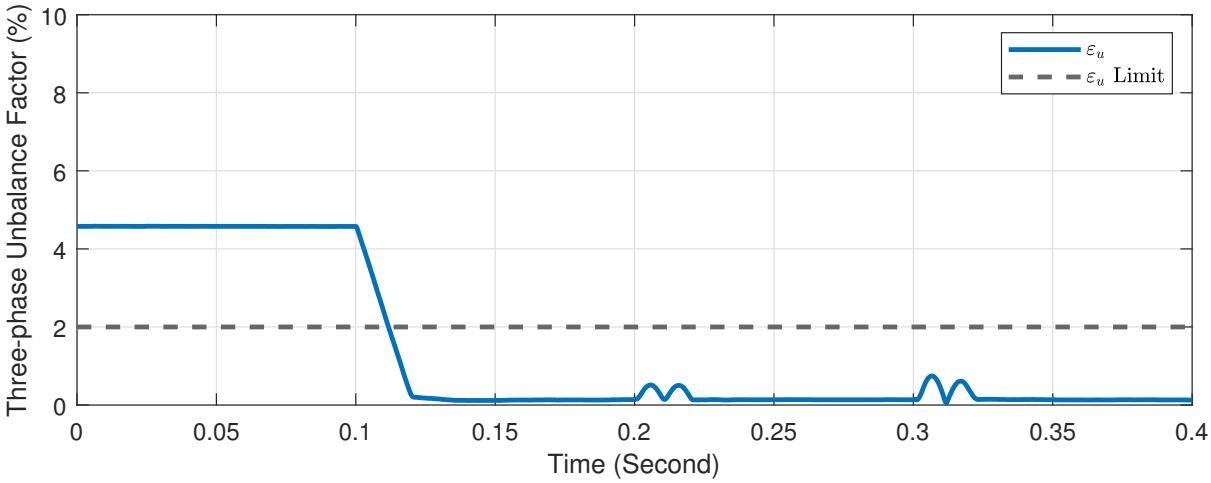

Figure 5.5: Simulation Result: Three-phase Unbalance Factor (Combined CTPSS)

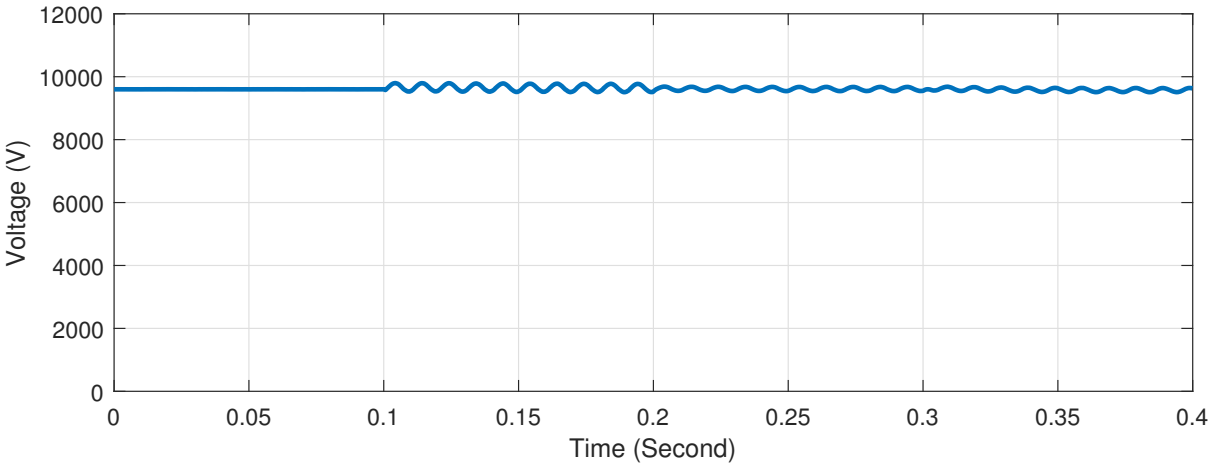

Figure 5.6: Simulation Result: DC Link Voltage in ADA (Combined CTPSS)

According to the simulation results, it can be observed that during $0 \sim 0.1$s, the CTPSS does not operate, i.e. it simulates a conventional hetero-phase TPSS with the traction power loaded on the TT , at which point the three-phase unbalance factor breaks the standard limit and reaches approximately 4.5%. Immediately afterwards, during the 0.1s ~ 0.2s stage, the CTPSS starts to compensate, and this compensation is complete. In this case, the TMT and TT each take half of the traction load power, at which point the three-phase unbalance factor is much weaker than the standard limit. This period is followed by a 0.2s ~ 0.3s stage in which the traction power is halved, at which point the system flexibly adapts to the new compensation values. In the 0.3s ~ 0.4s after this, the traction power switches to RBE mode, i.e. energy flows from the traction network to the grid, and the system also flexibly adapts the power.

The above tests show that the combined CTPSS in the simulation works as intended and can be flexibly adjusted to cope with all types of load, including the RBE scenario.

5.1.2 Simulation of HESS

Simulation models on HESS are also constructed in MATLAB/Simulink R2021a. The simulation parameters of the HESS part is aggregated in Table 5.3.

Table 5.3: Parameters Implemented in Simulation of HESS

Parameter	Value
Power Limit of BAT Array	$\pm 2\mathrm{MW}$
Power Limit of SC Array	$\pm 5\mathrm{MW}$
Inductance of DC-DC Converters	$4\mathrm{mH}$
Equivalent Rated Capacity of BAT Array	$300\mathrm{Ah}$
Equivalent Capacitance of SC Array	$500\mathrm{F}$
Nominal Voltage of BAT/SC Array	$1200\mathrm{V}$
Initial SOC of BAT/SC Array	50%

The overall simulation structure regarding HESS is presented clearly in Figure 5.7. A simulated DC power supply/load is placed on the HESS port, which has a shared connection between both the BAT array and SC array to simulate the various operating conditions of the HESS. The BAT array subsystem and the SC array subsystem, including the half-bridge bi-directional DC-DC converters, are exhibited in Figure 5.8 and Figure 5.9 respectively.

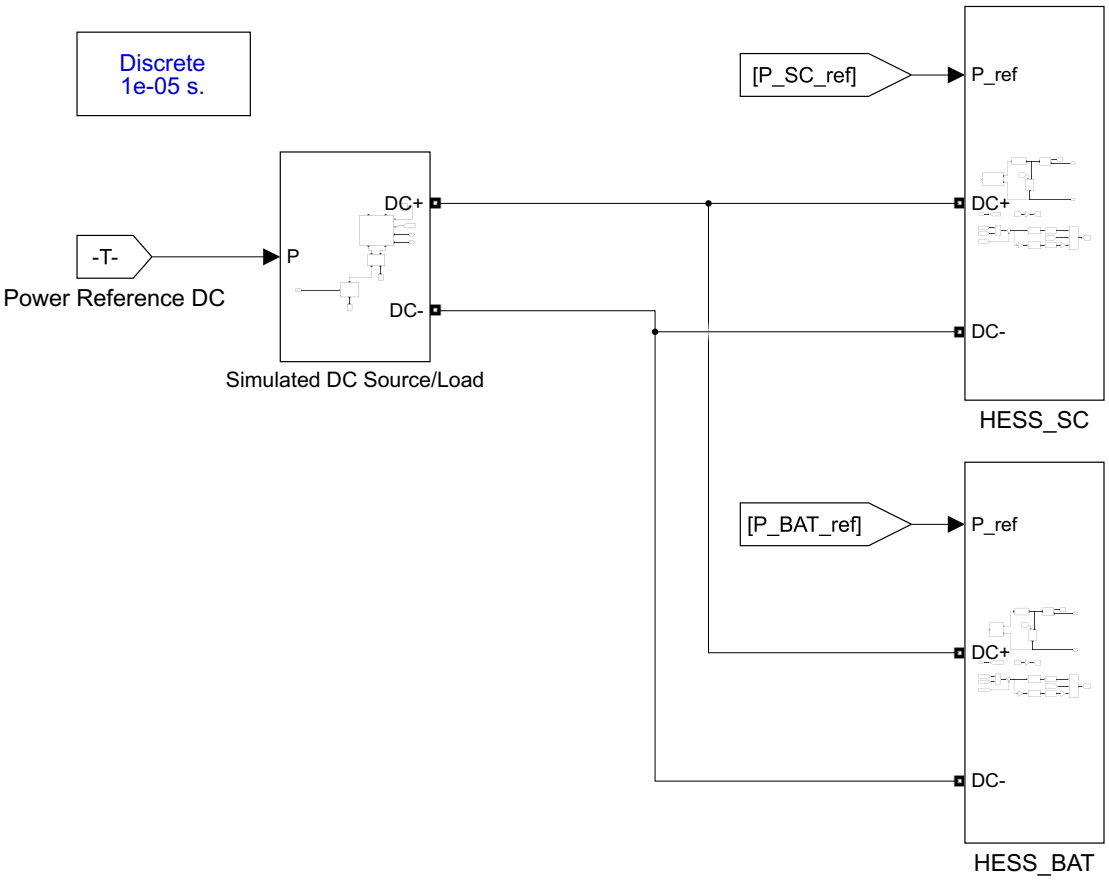

Figure 5.7: Schematic of HESS in Simulink

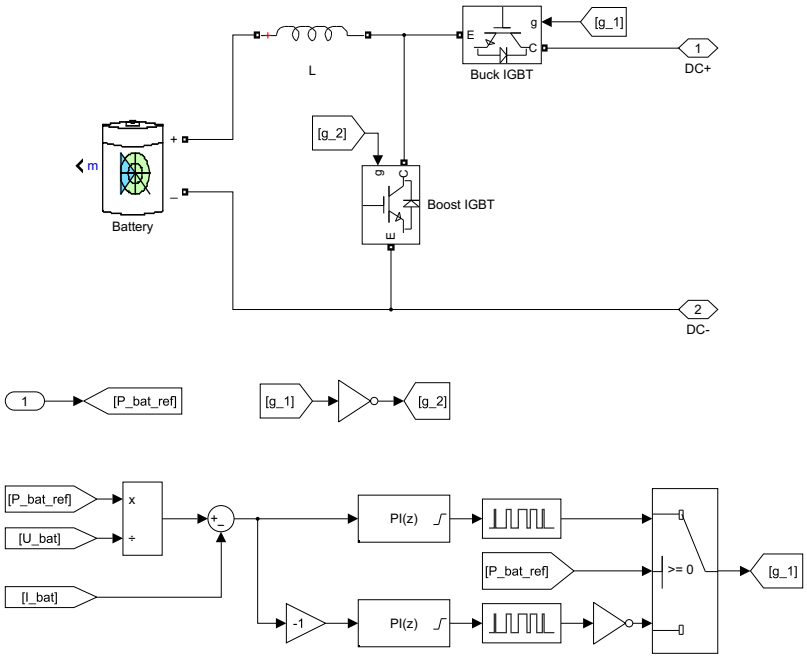

Figure 5.8: Schematic of HESS Battery Subsystem in Simulink

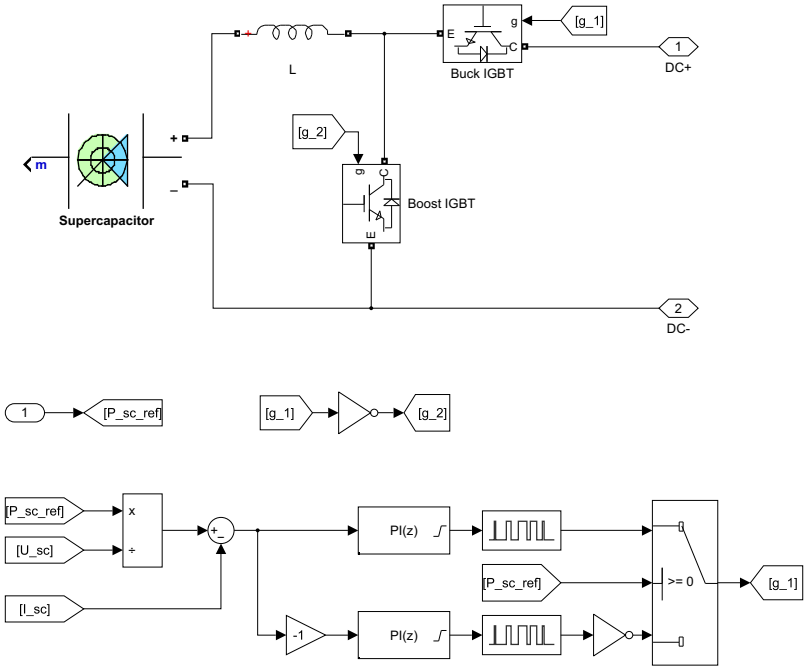

Figure 5.9: Schematic of HESS Supercapacitor Subsystem in Simulink

For the simulation of the HESS, the primary purpose is to verify that the individual energy storage units of the HESS can store and release energy properly and also to verify the power distribution capability. For the HESS, a highly fluctuating test power dataset of the virtual load-/source P_{HESS} was arranged. Four test objectives designed as $5\mathrm{MW}, 0\mathrm{MW}, -5\mathrm{MW}, -3\mathrm{MW}$ separated by 0.1s. The test results for the BAT array and the SC array are shown in Figure 5.10 and their SOC results are shown in Figure 5.11.

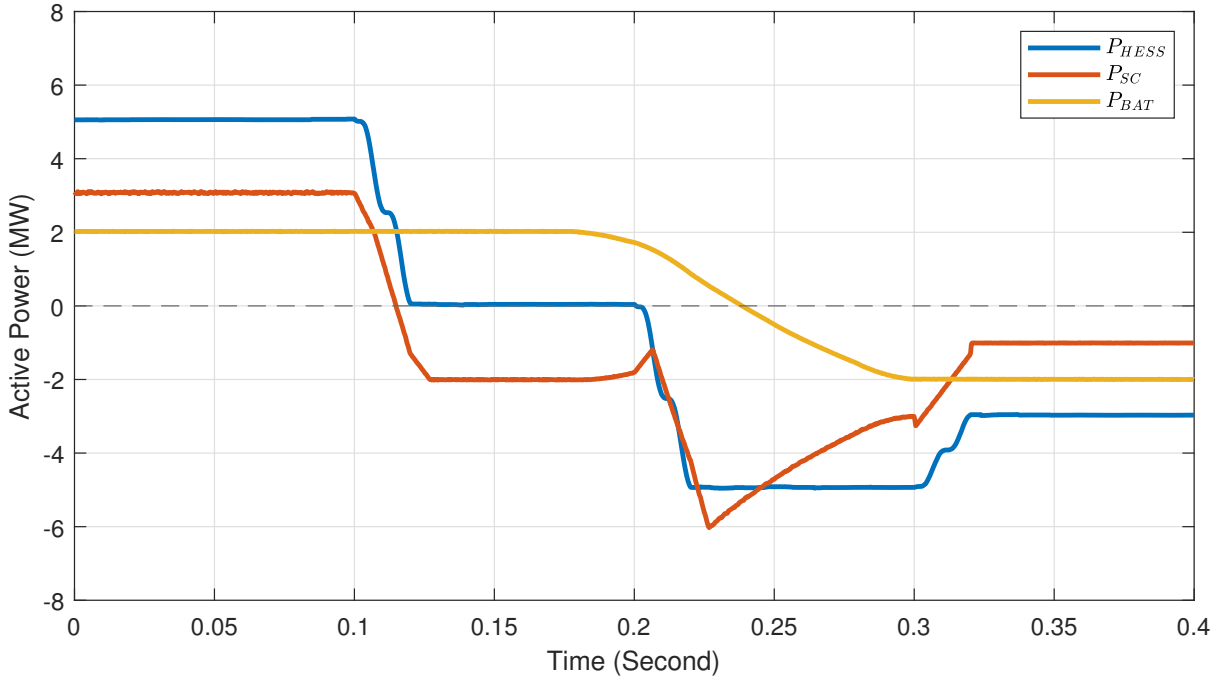

Figure 5.10: Simulation Result: Port Power (HESS)

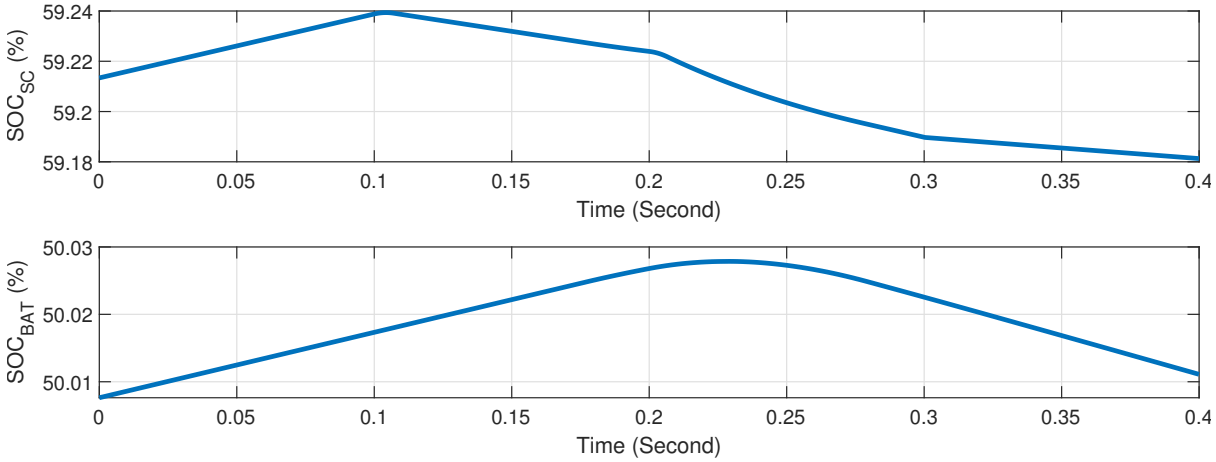

Figure 5.11: Simulation Result: SOC of Storage Arrays (HESS)

The above results show that the HESS can flexibly cope with loads and power sources while complying with the power limits. SOC simulations on SC and Li-ion BAT have also been successfully implemented. Furthermore, both the SOC curves and the power curves show that the two different energy storage medium, after power distribution, exhibit the desired power profile, i.e. the SC array carries the higher frequency varying power demand. In contrast, the

Li-ion BAT array carries the lower frequency power demand with a slower rate of change and does not exceed the power limit.

5.2 Control Strategy Verification

Both the combined CTPSS and HESS have been modelled and simulated to promising effect. A model of the HESCPSS was designed as the one shown in Figure 5.12. This system connects the combined CTPSS and HESS via a DC link in the ADA. The simulation is run by accepting a reference power signal from a source. It is necessary to remark that a virtual load is connected to the traction network to simulate the dynamic traction load and RBE. Besides, the complete control strategy logic was implemented in MATLAB/Simulink.

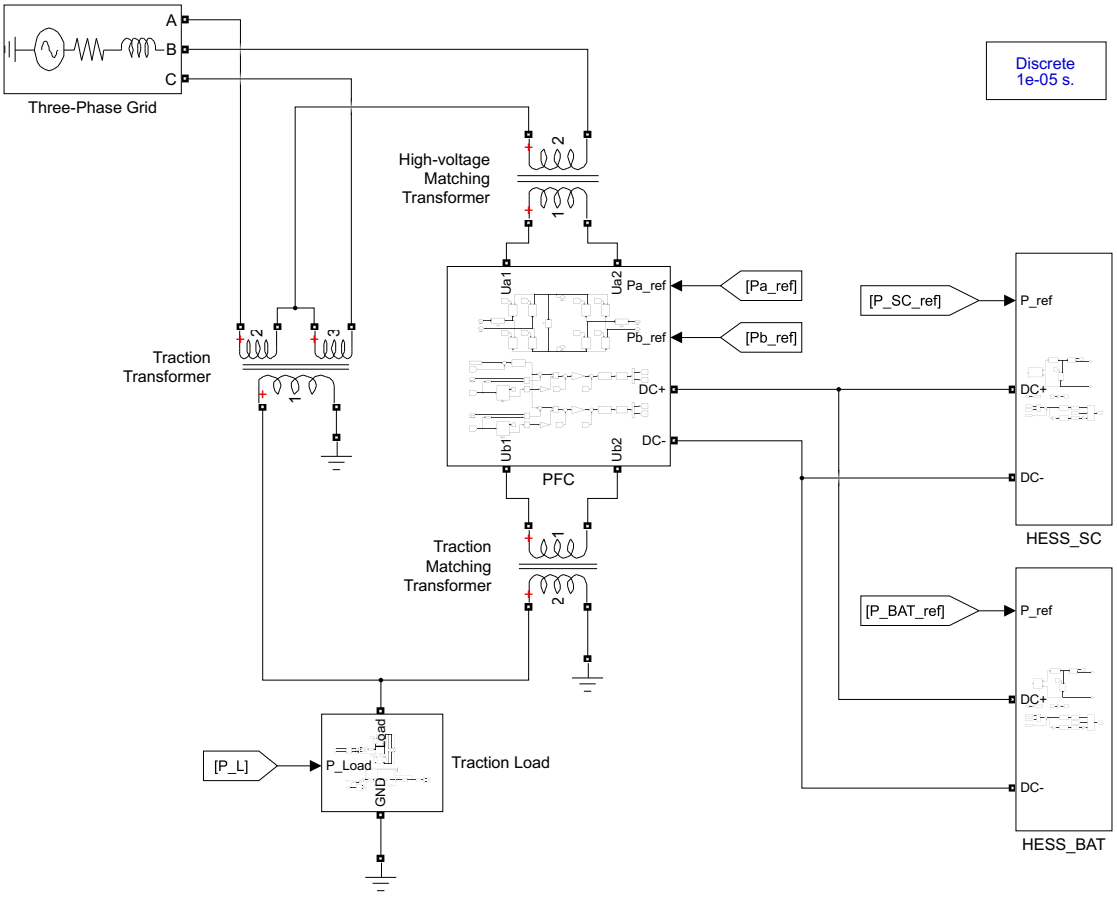

Figure 5.12: Schematic of HESCPSS in Simulink

Table 5.4: Parameters Applied in Control of HESCPSS

Parameter	Value
$\overline{P_{\mathrm{HESS}}}$	5MW
P_{RB}	$-$20MW
P_{TR}	16MW
P_{SG}	25MW
$\overline{\varepsilon_u}$	2%

In this simulation, in addition to the previously mentioned simulation parameters (Table 5.1 and Table 5.3), the parameters shown in Table 5.4 for the control strategy are also introduced. According to the calculations, the use of these parameters in each pattern does not cause the three-phase unbalance factor observed from the grid side to exceed the preset limit $\overline{\varepsilon_u}$.

Table 5.5: Test Objectives for Simulation of HESCPSS (0.2s each)

P_L Power Condition (MW)	Expected Pattern	Expected P_{TT} (MW)	Expected P_α (MW)	Expected P_{HESS} (MW)	Expected P_β (MW)
-25	RB (c)	-10	-10	5	-15
-15	RB (b)	-10	0	5	-5
-3	RB (a)	0	0	3	-3
3	TR (a)	3	3	3	0
12	TR (b)	12	5	5	0
20	SG (a)	10	10	0	10
35	SG (b)	15	15	-5	20

The corresponding test objectives are arranged for each operating pattern, as shown in Table 5.13. The only data entered into the simulation model is the load power data P_L. For each test objective, there is a set of desired operating pattern and desired TT power, CPD α port power, β port power and HESS net power. The values of these expectations were determined using the conclusions in Table 3.1.

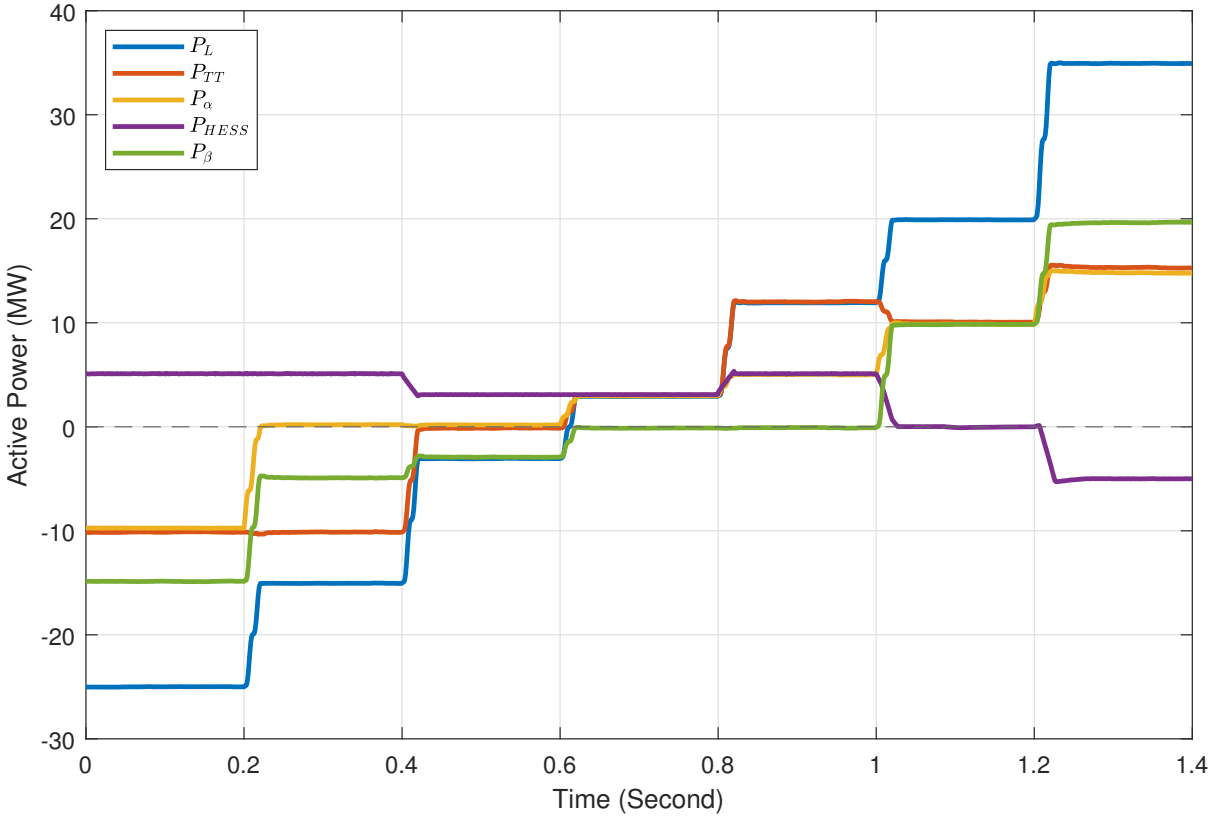

Figure 5.13: Simulation Result: Port Power (HESCPSS)

As can discover in Figure 5.13, the power flows on the individual links are as required and the system behaves as expected. This shows the correctness of the overall system simulation.

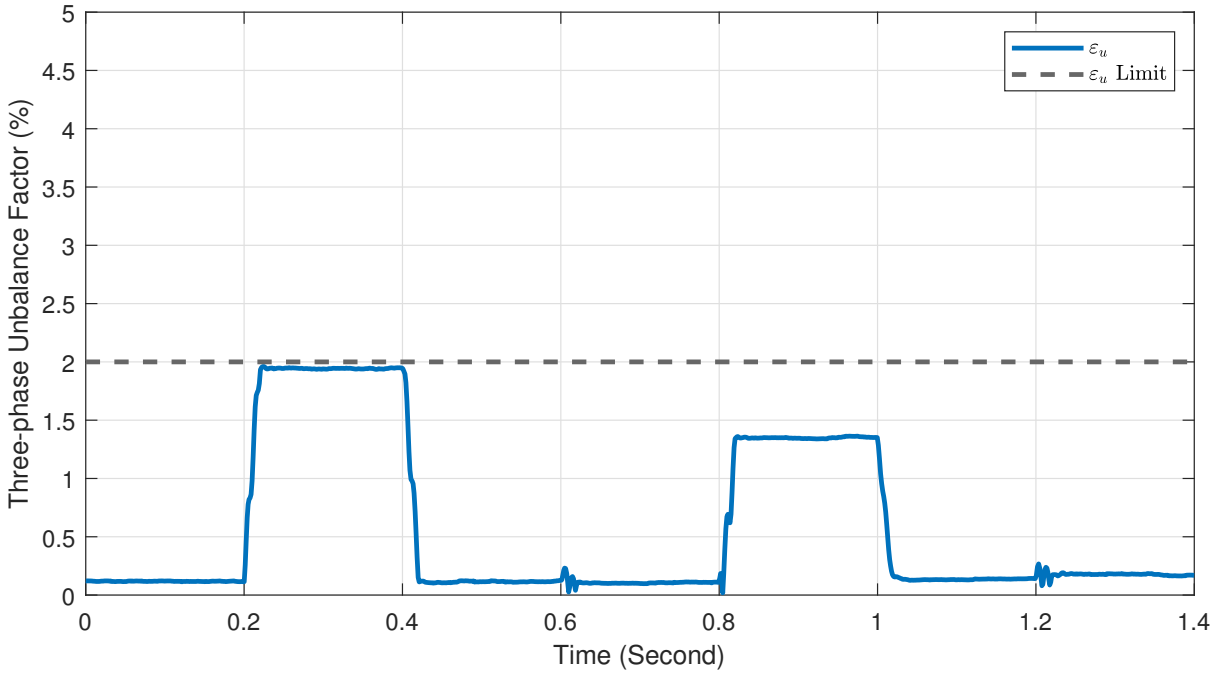

Figure 5.14: Simulation Result: Three-phase Unbalance Factor (HESCPSS)

Figure 5.14 presents the three-phase unbalance factor on the grid side calculated from the short-circuit capacity S_{sc}, and it can be seen that the HESCPSS can be fully compliant to the limitation $\overline{\varepsilon_u}$. Furthermore, the system is capable of achieving accurate, marginal compensation, e.g. in the case of $0.2\text{s} \sim 0.4\text{s}$.

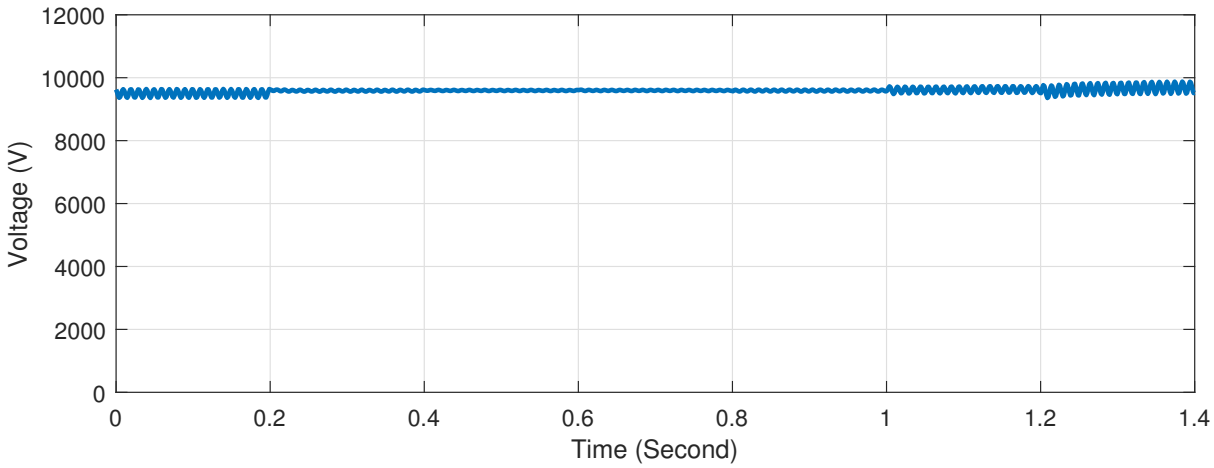

Figure 5.15: Simulation Result: DC Link Voltage in ADA (HESCPSS)

The DC link related results are displayed, Figure 5.15 for DC link voltage in ADA, also the interface for HESS; Figure 5.16 for the power of SC and Li-ion BAT; Figure 5.17 for the SOC of SC array and Li-ion BAT array. From these figures, it is discernable that the DC link of the ADA maintains a relatively stable voltage under all operating conditions. In addition, the power distribution within the HESS has been successfully implemented.

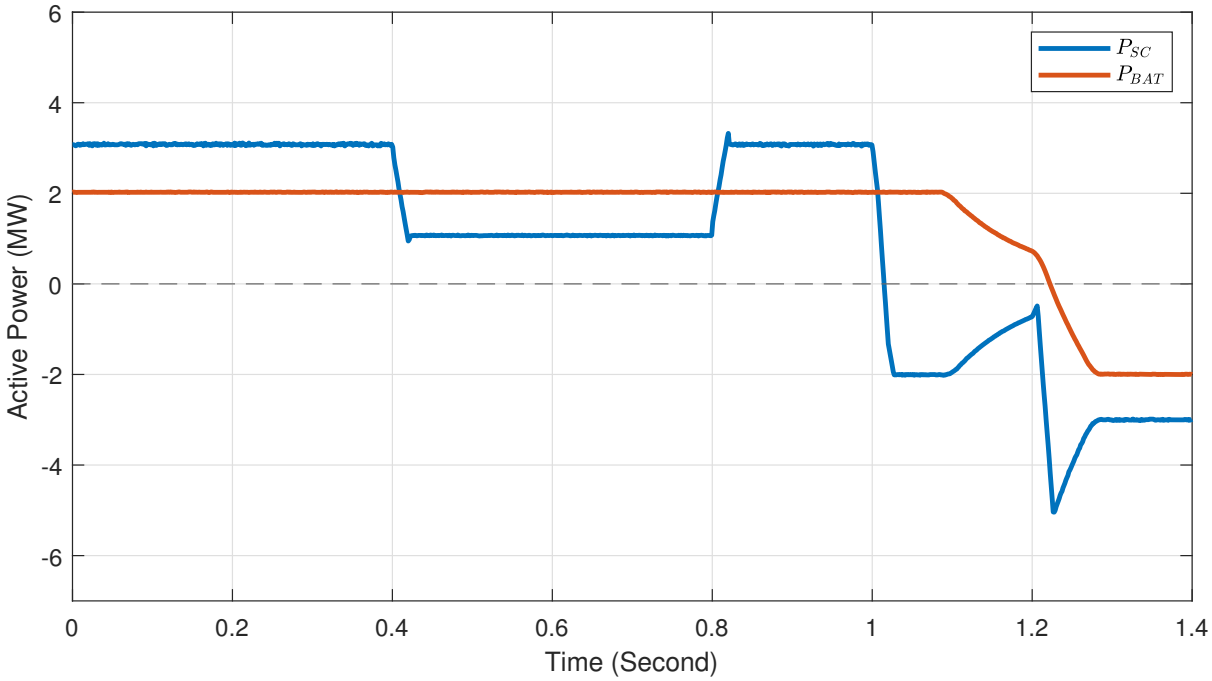

Figure 5.16: Simulation Result: HESS Power (HESCPSS)

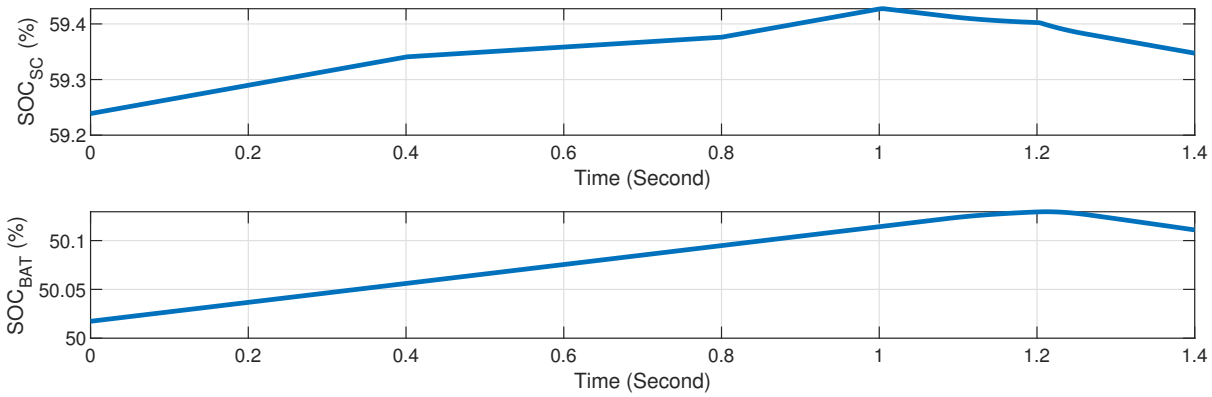

Figure 5.17: Simulation Result: SOC of Storage Arrays (HESCPSS)

5.3 Case Study

Based on the previously implemented simulation model, the proposed model and control strategy should be simulated and validated with actual load data obtained from the traction substations directly. Figure 5.18 shows the real intra-day load data for a traction substation. It should be heeded that this data contains only active power as previously practised, and since the data comes from a conventional TPSS, which contains two supply arms for two electrical split phases, the data used in this simulation is the sum of the active power of the two supply arms.

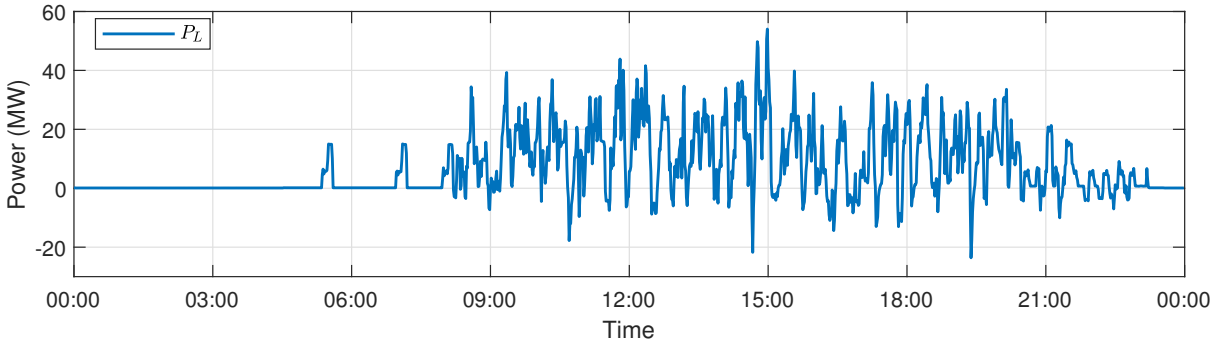

Figure 5.18: Load Power Data in Case Study

By applying the control strategy parameters in Table 5.4, and the parameters previously used for the HESCPSS simulation, the following results can be obtained:

The time share profile of each operating pattern can be derived as shown in Table 5.6, and as can be found in Figure 5.19, the power of each port of the HESCPSS is controlled according to the specified control strategy. It is also explicit that in many cases, both TT and CPD supply the load simultaneously, which ensures that the three-phase unbalance factor can be restricted within limits. In addition, the power distribution strategy regarding the HESS has been validated, while the power limits for the two different ESSs are also in effect.

By integrating the power of the ports in Figure 5.19, the intra-day power consumption and the RBE amount can be obtained, as shown in Table 5.7. It can be seen from the amount of power taken and fed into the grid that the proposed HESCPSS has a much improved utilisation of the RBE. At the same time, the SG patterns provided a smooth reduction of the peak power consumption, resulting in a reduction of the demand power.

It is important to mention that the calculation of the demand power is based on a sliding average over a 15 minute window.

$$P_{\text{demand,max}} = \max\left[\sum_{t}^{t+14} \frac{P_{\text{TT}} + P_{\alpha}}{15}\right] \qquad \forall t = 1, 2, \ldots, card(T) - 14 \tag{5.1}$$

where T is a time interval set that contains all minutes in a day, and therefore $card(T)$ is equal to 1440.

At the same time, the HESS has been effectively simulated, and the state of charge of the SC array and the Li-ion BAT array can be obtained from the simulation results, which are shown in Figure 5.20. By combining the power data and SOC data, it can be discerned that the self-discharge characteristics, power distribution capability, SOC protection and charge/discharge simulation of the HESS have all been effectively realised.

Based on the data obtained from the simulation and the short-circuit capacity of the grid S_{sc}, the grid-side three-phase unbalance factor of the conventional TPSS and the HESCPSS proposed in this project can be derived readily, and the results are indicated in Figure 5.21. It can be seen that with the application of the HESCPSS and its control strategy, i.e. with compensation, the three-phase unbalance factor is very effectively and strictly controlled compared to the case of the conventional TPSS. At all times of the day, the three-phase unbalance did not exceed the design limits $\overline{\varepsilon_u}$.

Table 5.6: Simulation Result: Intra-day Time Share of Operating Patterns in Case Study

Pattern	Time Percentage
RB (c)	0.00%
RB (b)	3.89%
RB (a)	8.40%
TR (a)	45.63%
TR (b)	21.53%
SG (a)	12.36%
SG (b)	8.06%

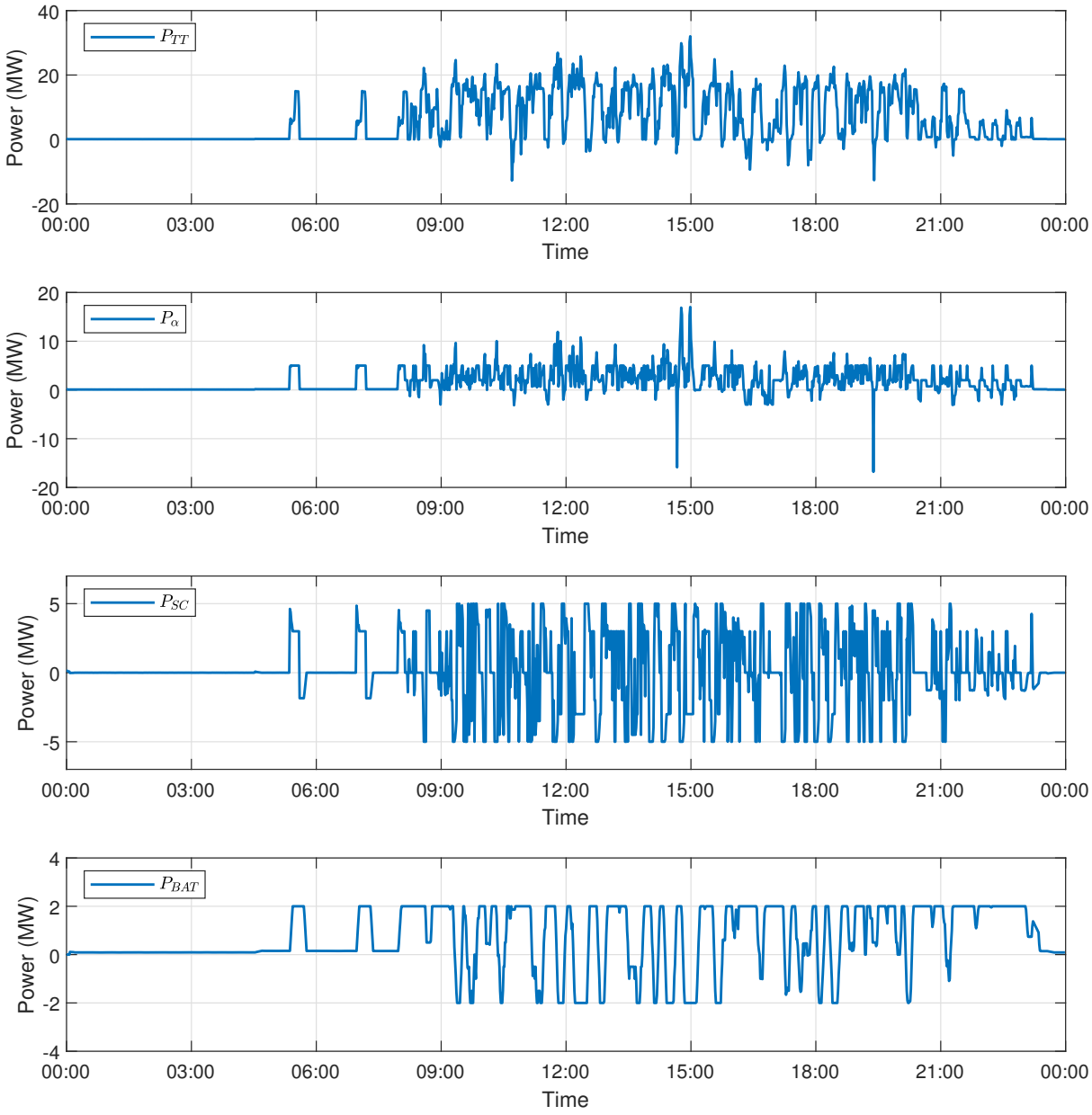

Figure 5.19: Simulation Result: Port Power in Case Study

Table 5.7: Simulation Result: Energy Consumption Comparison in Case Study

Quantity	Tradition TPSS	Proposed HESCPSS	Reduction Rate
Load Energy Consumption	$181,080\text{kWh}$	$181,080\text{kWh}$	-
Energy Drawn on the Grid	$181,080\text{kWh}$	$147,790\text{kWh}$	-23.28%
Energy Fed back to the Grid	0	$8,869\text{kWh}$	(net energy)
Peak of Demand Power	32.8251MW	27.9371MW	-14.89%

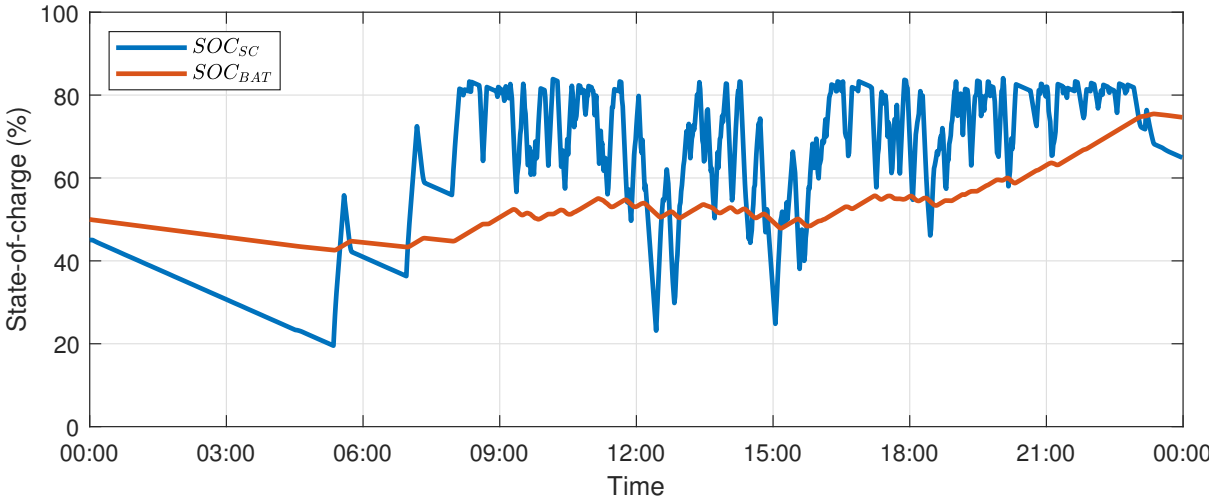

Figure 5.20: Simulation Result: SOC of Storage Arrays in Case Study

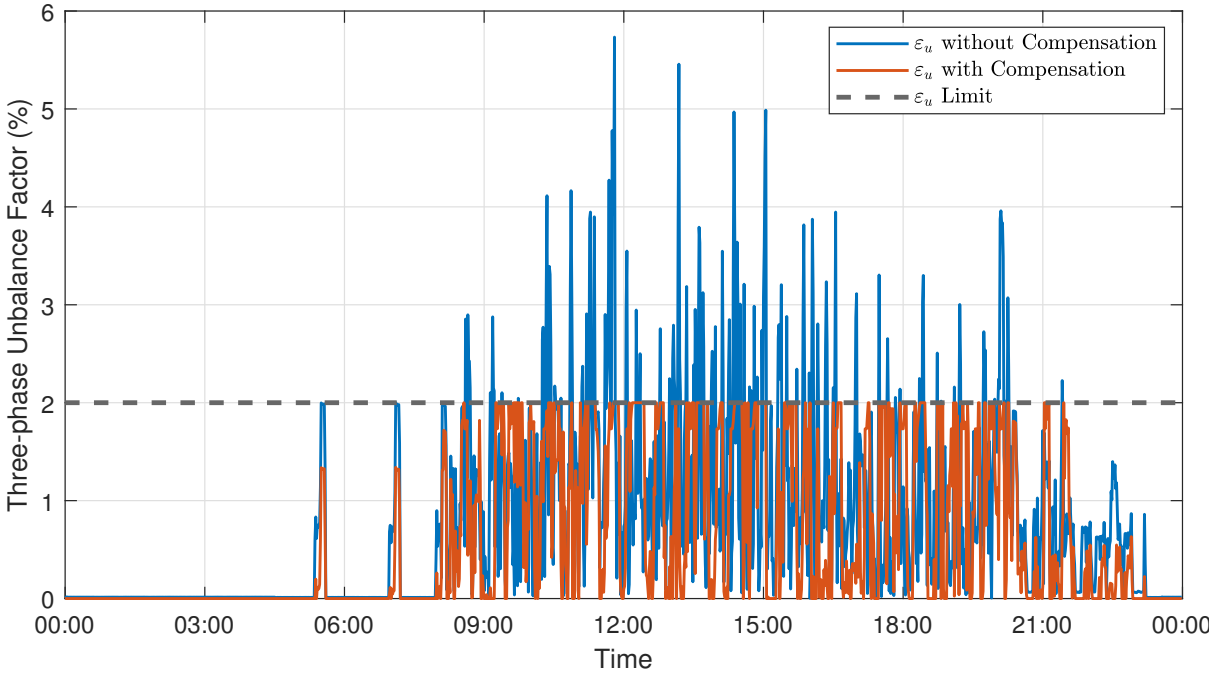

Figure 5.21: Simulation Result: Three-phase Unbalance Factor of HESCPSS in Case Study

Chapter 6

Conclusions

After identifying the application context, this project taps into the current state of the art in the areas of traction power supply system (TPSS), high-speed railway (HSR) and energy storage system (ESS). It then identifies and proposes a novel hybrid energy storage co-phase power supply system (HESCPSS) with combined co-phase traction power supply system (CTPSS) and hybrid energy storage system (HESS) as the main components. The study shows that the HESCPSS can effectively achieve power quality management, regenerative braking energy (RBE) utilisation enhancement and system power capacity optimisation, thus ensuring safe, reliable and efficient operation of the electrified railway.

Based on the actual completion of the project, it can be determined that the following objectives were achieved:

- The principle of the combined CTPSS and HESS has been studied and validated.
- The structure of the HESCPSS is clarified, where the structure of the AC-DC-AC converter (ADA) of the combined CTPSS is also specified, as is the structure of the HESS.
- The operating patterns of the HESCPSS under various load conditions are analysed in detail, and the detailed power allocations for each operating patterns are derived.
- Control methods that can be used for their power electronic converters are studied based on the combined CTPSS and HESS characteristics, respectively. An overall system coordination control strategy is hence built based on the operating patterns of the HESCPSS.
- In MATLAB/Simulink R2021a, the system structure and control strategy of HESCPSS are correctly implemented. Simulations have proven that individual parts of the HESCPSS, as a whole, and the control strategy work as expected.
- The simulation results confirmed that the system operation could ensure excellent dynamic versatility and support the required grid-side power quality under every operating condition.

However, due to the limited time available for the project, the following deficiencies and remaining issues were identified in the development of this project:

- The determination of thresholds in control strategies and the capacity configuration of the various components of the system have not been explored in detail in this project,

primarily because their calculation relies heavily on actual engineering practice and target costs, which are often complex to model and beyond the scope of this project's work.

- Only one traction substation has been considered for this project, whereas in practical engineering applications, it is common for multiple substations to be jointly dispatched and controlled.
- This project has only carried out computational analysis and computer-based simulations of the proposed system and control theory, and has not designed and built a physical prototype or some equivalent alternative validation device. This is mainly due to the complexity of the model, the duration of the project and the budget.

For potential future research, the above issues can be explored in depth on the results of this project.

Overall, the proposed HESCPSS, simultaneously, manages the power quality problems, improves the utilisation of the RBE and optimises the total system power consumption. The proposed system structure and control strategy in this project can provide practical scientific assistance for electrified railways and promote the engineering application of hybrid energy storage integrated co-phase traction power supply systems.

Glossary

ADA	AC-DC-AC Converter
APC	Active Power Compensation Device
BAT	Battery (for most cases in this project, specially for lithium-ion battery)
CPD	Co-phase Power Supply Device
CTPSS	Co-phase Traction Power Supply System
ESS	Energy Storage System
HESCPSS	Hybrid Energy Storage Co-phase Power Supply System
HESS	Hybrid Energy Storage System
HMT	High-voltage Matching Transformer
HSR	High-Speed Railway
RB	Regenerative Braking Pattern
RBE	Regenerative Braking Energy
SC	Supercapacitor
SG	Demand Surge Smoothing Pattern
SOC	State-Of-Charge
TMT	Traction Matching Transformer
TPSS	Traction Power Supply System
TR	Demand Trough Smoothing Pattern
TT	Traction Transformer

References

[1] J. Li, X. Li, W. Deng, Z. Xu, Q. Liu, and Y. Zhang, "Study on power systems transient stability considering traction power supply system measurement-based load model," in *2011 International Conference on Advanced Power System Automation and Protection*, vol. 2, 2011, pp. 1430–1434.

[2] S. M. Mousavi Gazafrudi, A. Tabakhpour Langerudy, E. F. Fuchs, and K. Al-Haddad, "Power quality issues in railway electrification: A comprehensive perspective," *IEEE Transactions on Industrial Electronics*, vol. 62, no. 5, pp. 3081–3090, 2015.

[3] T. A. Kneschke, "Control of utility system unbalance caused by single-phase electric traction," *IEEE Transactions on Industry Applications*, vol. IA-21, no. 6, pp. 1559–1570, Nov 1985.

[4] B. Busco, P. Marino, M. Porzio, R. Schiavo, and F. Vasca, "Digital control and simulation for power electronic apparatus in dual voltage railway locomotive," *IEEE Transactions on Power Electronics*, vol. 18, no. 5, pp. 1146–1157, 2003.

[5] Z. He, Z. Zheng, and H. Hu, "Power quality in high-speed railway systems," *International Journal of Rail Transportation*, vol. 4, no. 2, pp. 71–97, 2016. [Online]. Available: https://doi.org/10.1080/23248378.2016.1169228

[6] S. Chen, R. . Li, and P. Hsi, "Traction system unbalance problem-analysis methodologies," *IEEE Transactions on Power Delivery*, vol. 19, no. 4, pp. 1877–1883, Oct 2004.

[7] V. Matta and G. Kumar, "Unbalance and voltage fluctuation study on ac traction system," in *2014 Electric Power Quality and Supply Reliability Conference (PQ)*, 2014, pp. 303–308.

[8] N. Dai, M. Wong, K. Lao, and C. Wong, "Modelling and control of a railway power conditioner in co-phase traction power system under partial compensation," *IET Power Electronics*, vol. 7, no. 5, pp. 1044–1054, May 2014.

[9] Q. Wang, J. Lu, Q. Wang, and J. Duan, "Transient overvoltage study of auto-passing neutral section in high-speed railway," in *2017 IEEE Transportation Electrification Conference and Expo, Asia-Pacific (ITEC Asia-Pacific)*, 2017, pp. 1–5.

[10] C. Huang, C. Wu, Y. Chuang, S. Peng, J. Yen, and M. Han, "Loading characteristics analysis of specially connected transformers using various power factor definitions," *IEEE Transactions on Power Delivery*, vol. 21, no. 3, pp. 1406–1413, 2006.

[11] H. Kuo and T. Chen, "Rigorous evaluation of the voltage unbalance due to high-speed railway demands," *IEEE Transactions on Vehicular Technology*, vol. 47, no. 4, pp. 1385–1389, 1998.

[12] S. Huang and B. Chen, "Harmonic study of the le blanc transformer for taiwan railway's electrification system," *IEEE Transactions on Power Delivery*, vol. 17, no. 2, pp. 495–499, 2002.

[13] G. Liu, Y. Zhou, and J. Yao, "Study of requirements and equivalent circuit of new balance transformer," *Proceedings-Chinese Society for Electrical Engineering*, vol. 19, pp. 84–88, 1999.

[14] W. Mingli, F. Yu, and X. Chengshan, "Study on operation characteristics and equivalent model of scott connection traction transformer," *Transactions of China Electrotechnical Society*, vol. 18, no. 4, pp. 75–80, 2003.

[15] Z. Shu, S. Xie, and Q. Li, "Development and implementation of a prototype for co-phase traction power supply system," in *2010 Asia-Pacific Power and Energy Engineering Conference*, March 2010, pp. 1–4.

[16] L. Min and X. Mou, "Simulation analysis of railway co-phase power supply system based on inequilateral scott connection transformer," in *2018 5th IEEE International Conference on Cloud Computing and Intelligence Systems (CCIS)*, 2018, pp. 1066–1071.

[17] Z. Shu, S. Xie, and Q. Li, "Single-phase back-to-back converter for active power balancing, reactive power compensation, and harmonic filtering in traction power system," *IEEE Transactions on Power Electronics*, vol. 26, no. 2, pp. 334–343, 2011.

[18] Q. Li, W. Liu, Z. Shu, S. Xie, and F. Zhou, "Co-phase power supply system for hsr," in *2014 International Power Electronics Conference (IPEC-Hiroshima 2014 - ECCE ASIA)*, May 2014, pp. 1050–1053.

[19] A. González-Gil, R. Palacin, and P. Batty, "Sustainable urban rail systems: Strategies and technologies for optimal management of regenerative braking energy," *Energy Conversion and Management*, vol. 75, pp. 374–388, 2013. [Online]. Available: https://www.sciencedirect.com/science/article/pii/S0196890413003518

[20] Z. Tian, P. Weston, N. Zhao, S. Hillmansen, C. Roberts, and L. Chen, "System energy optimisation strategies for metros with regeneration," *Transportation Research Part C: Emerging Technologies*, vol. 75, pp. 120–135, 2017. [Online]. Available: https://www.sciencedirect.com/science/article/pii/S0968090X16302522

[21] A. Siemens, "Increasing energy efficiency: Optimized traction power supply in mass transit systems," 2011.

[22] R. Teymourfar, B. Asaei, H. Iman-Eini, and R. Nejati fard, "Stationary super-capacitor energy storage system to save regenerative braking energy in a metro line," *Energy Conversion and Management*, vol. 56, pp. 206 – 214, 2012. [Online]. Available: http://www.sciencedirect.com/science/article/pii/S0196890411003372

[23] H. Sameshima, M. Ogasa, and T. Yamamoto, "On-board characteristics of rechargeable lithium ion batteries for improving energy regenerative efficiency," *Quarterly Report of RTRI*, vol. 45, no. 2, pp. 45–52, 2004.

[24] L. Hou, S. Zhang, Y. Wei, X. Li, Q. Jiang, M. Li, and W. Li, "A novel dc traction power supply system based on the modular multilevel converter suitable for energy feeding and de-icing," *CSEE Journal of Power and Energy Systems*, pp. 1–10, 2020.

[25] Y. Mochinaga and T. Uzuka, "Development of single phase feeding power conditioner for shinkansen depots," *Quarterly Report of RTRI*, vol. 41, no. 4, pp. 154–158, 2000.

[26] M. Ando, Y. Hisamizu, and Y. Nakamichi, "Development of power feeding transformer for shinkansen suitable for extra high voltage substation," *RTRI REPORT*, vol. 16, no. 6, 2002.

[27] S. Li, S. Wu, P. Yang, and S. He, "Research on sychronverter-based regenerative braking energy feedback system of urban rail trains," in *2019 14th IEEE Conference on Industrial Electronics and Applications (ICIEA)*, 2019, pp. 1765–1770.

[28] J. Chen, H. Hu, K. Wang, W. Wei, and Z. He, "A method for evaluating regenerative energy of traction power supply system of high speed railway considering train working diagram," *China Railway Science*, 2019.

[29] H. Chen, T. N. Cong, W. Yang, C. Tan, Y. Li, and Y. Ding, "Progress in electrical energy storage system: A critical review," *Progress in Natural Science*, vol. 19, no. 3, pp. 291 – 312, 2009. [Online]. Available: http://www.sciencedirect.com/science/article/pii/S100200710800381X

[30] H. Ibrahim, A. Ilinca, and J. Perron, "Energy storage systems—characteristics and comparisons," *Renewable and Sustainable Energy Reviews*, vol. 12, no. 5, pp. 1221 – 1250, 2008. [Online]. Available: http://www.sciencedirect.com/science/article/pii/S1364032107000238

[31] M. Khodaparastan, A. A. Mohamed, and W. Brandauer, "Recuperation of regenerative braking energy in electric rail transit systems," *IEEE Transactions on Intelligent Transportation Systems*, vol. 20, no. 8, pp. 2831–2847, 2019.

[32] M. M. Rahman, A. O. Oni, E. Gemechu, and A. Kumar, "Assessment of energy storage technologies: A review," *Energy Conversion and Management*, vol. 223, p. 113295, 2020. [Online]. Available: https://www.sciencedirect.com/science/article/pii/S0196890420308347

[33] M. Choi, S. Kim, and S. Seo, "Energy management optimization in a battery/supercapacitor hybrid energy storage system," *IEEE Transactions on Smart Grid*, vol. 3, no. 1, pp. 463–472, 2012.

[34] M. Ding and J. Wu, "A novel control strategy of hybrid energy storage system for wind power smoothing," *Electric Power Components and Systems*, vol. 45, no. 12, pp. 1265–1274, 2017. [Online]. Available: https://doi.org/10.1080/15325008.2017.1346004

[35] P. Zhang, X. Ma, and K. She, "A novel power-driven fractional accumulated grey model and its application in forecasting wind energy consumption of china," *PloS one*, vol. 14, no. 12, p. e0225362, 2019.

[36] H. Xie, Y. Liu, Z. Cheng, and Y. Cheng, "Optimal hybrid energy storage sizing for co-phase traction power supply system based on grey wolf optimizer," in *2020 15th IEEE Conference on Industrial Electronics and Applications (ICIEA)*, 2020, pp. 425–430.

[37] C. Huang, Y. Xie, Y. Liu, and M. Chen, "Energy management of co-phase traction power supply system considering pv and hybrid energy access based on information gap decision theory," in *2020 IEEE Sustainable Power and Energy Conference (iSPEC)*, 2020, pp. 238–244.

[38] Y. Zhao, N. Dai, and B. An, "Application of three-phase modular multilevel converter (mmc) in co-phase traction power supply system," in *2014 IEEE Conference and Expo Transportation Electrification Asia-Pacific (ITEC Asia-Pacific)*, 2014, pp. 1–6.

[39] Q. Li, "New generation traction power supply system and its key technologies for electrified railways," *Journal of Modern Transportation*, vol. 23, no. 1, pp. 1–11, 2015.

[40] N. Zhang, D. Sutanto, and K. M. Muttaqi, "A review of topologies of three-port dc–dc converters for the integration of renewable energy and energy storage system," *Renewable and Sustainable Energy Reviews*, vol. 56, pp. 388–401, 2016. [Online]. Available: https://www.sciencedirect.com/science/article/pii/S1364032115013465

[41] J. W. Dixon and Boon-Teck Ooi, "Indirect current control of a unity power factor sinusoidal current boost type three-phase rectifier," *IEEE Transactions on Industrial Electronics*, vol. 35, no. 4, pp. 508–515, 1988.

[42] X. Chuan, Z. Liu, S. Yao, and G. Zhang, "Decoupling predictive current control for traction line-side converter in high-speed railway," in *2016 12th World Congress on Intelligent Control and Automation (WCICA)*, 2016, pp. 1781–1785.